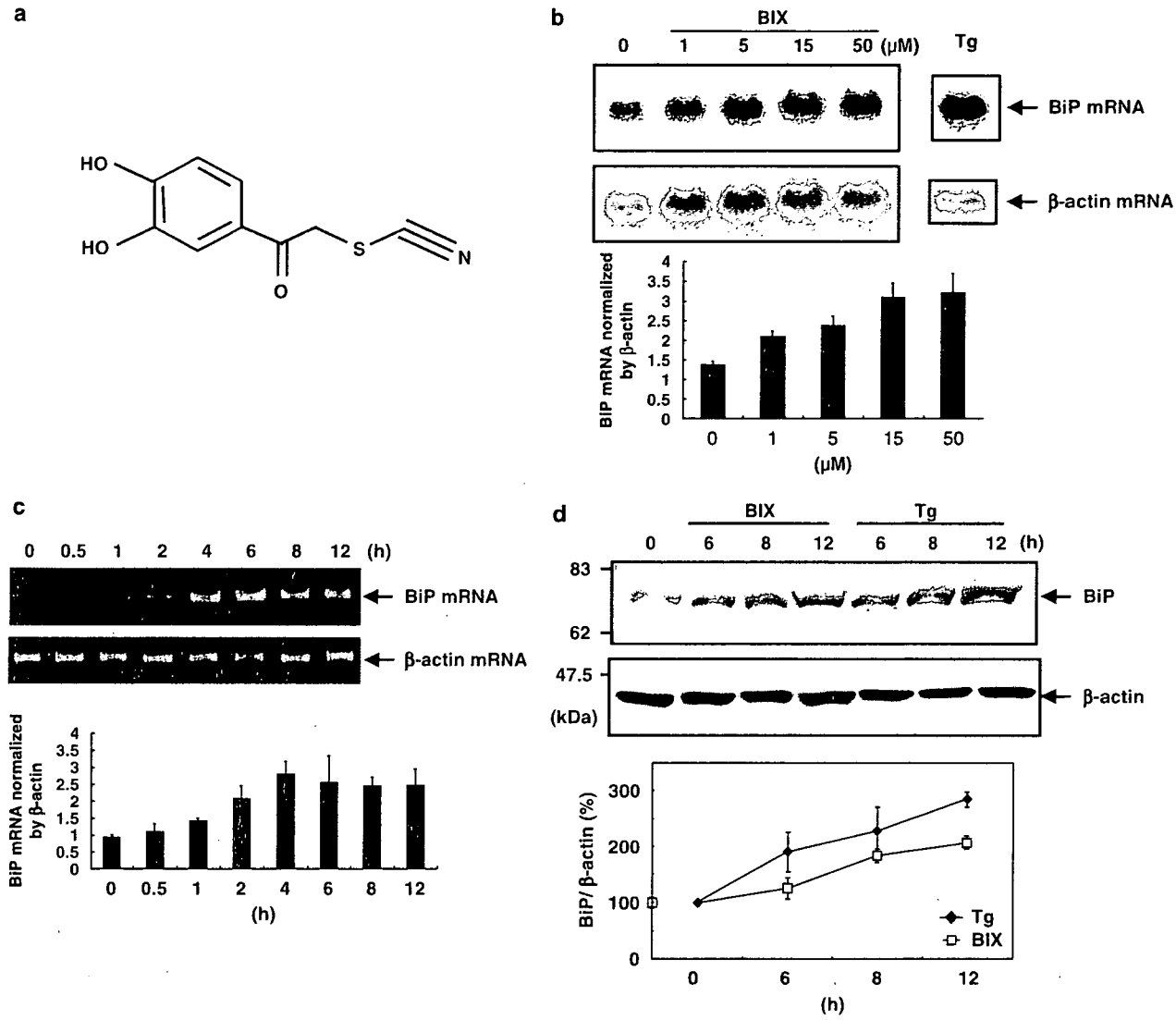

Figure 1 BIX induces BiP. (**a**) The structure of BIX (1-(3,4-dihydroxyphenyl)-2-thiocyanate-ethanone). (**b**) Dose-dependent induction of BiP mRNA in SK-N-SH cells after 6 h of treatment with BIX is shown by northern blot (upper panel) and real-time PCR (lower panel); values are means ± S.D. from three independent experiments. The induction of BiP mRNA by Tg is shown as a positive control. β-Actin mRNA is shown as an internal control. (**c**) The time course of BiP mRNA induction in cells treated with BIX is shown by semiquantitative RT-PCR (upper panel) and real-time PCR (lower panel); values are means ± S.D. from three independent experiments. The level of BiP mRNA peaked in 4 h and kept until 6 h after treatment with BIX at 5 μM, with a subsequent reduction after this point. (**d**) A time-dependent induction of BiP protein in SK-N-SH cells treated with 5 μM BIX or 1 μM Tg is detected by immunoblot and quantified by densitometry. Values are means ± S.D. from three independent experiments

finding supports the results shown in Figure 1c and suggests that the effects of BIX on BiP induction are transient and that BiP mRNA reverts to basal levels. Therefore, induction of BiP by BIX might be caused by a mechanism different to that used by ER stressors such as Tg and Tm, and the BIX-responsive element(s) might be included in the 132 bp BiP promoter region. Within this 132 bp region, there are three ER stress response elements (ERSEs) (Figure 3a). Subsequently, we carried out the reporter assay using an ERSE mut (132)-pGL3 plasmid (Figure 3a) to confirm whether or not these ERSEs are involved in the induction of BiP by BIX. BiP (132)-pGL3 or ERSE mut (132)-pGL3 was transfected into SK-N-SH cells, and the cells were treated with 5 μM BIX for 6 h. The reporter activities in cells transfected with BiP (132)-pGL3 were increased ~4-fold by BIX. On the other hand, induction of reporter activity was not observed in cells transfected with ERSE mut (132)-pGL3 (Figure 3c). This result suggests that ERSEs are involved in the induction of BiP by BIX.

Next, to examine whether three major transducers of the ER stress response, namely PERK, IRE1, and ATF6, affect the induction of BiP by BIX, we analyzed the expression of BiP in knockout/knockdown mouse embryonic fibroblasts (MEFs) lacking each transducer (Figure 3d). In PERK-deficient MEFs and IRE1α/β double-knockout MEFs, BiP mRNA was induced by BIX to a similar level to that seen in wild-type cells

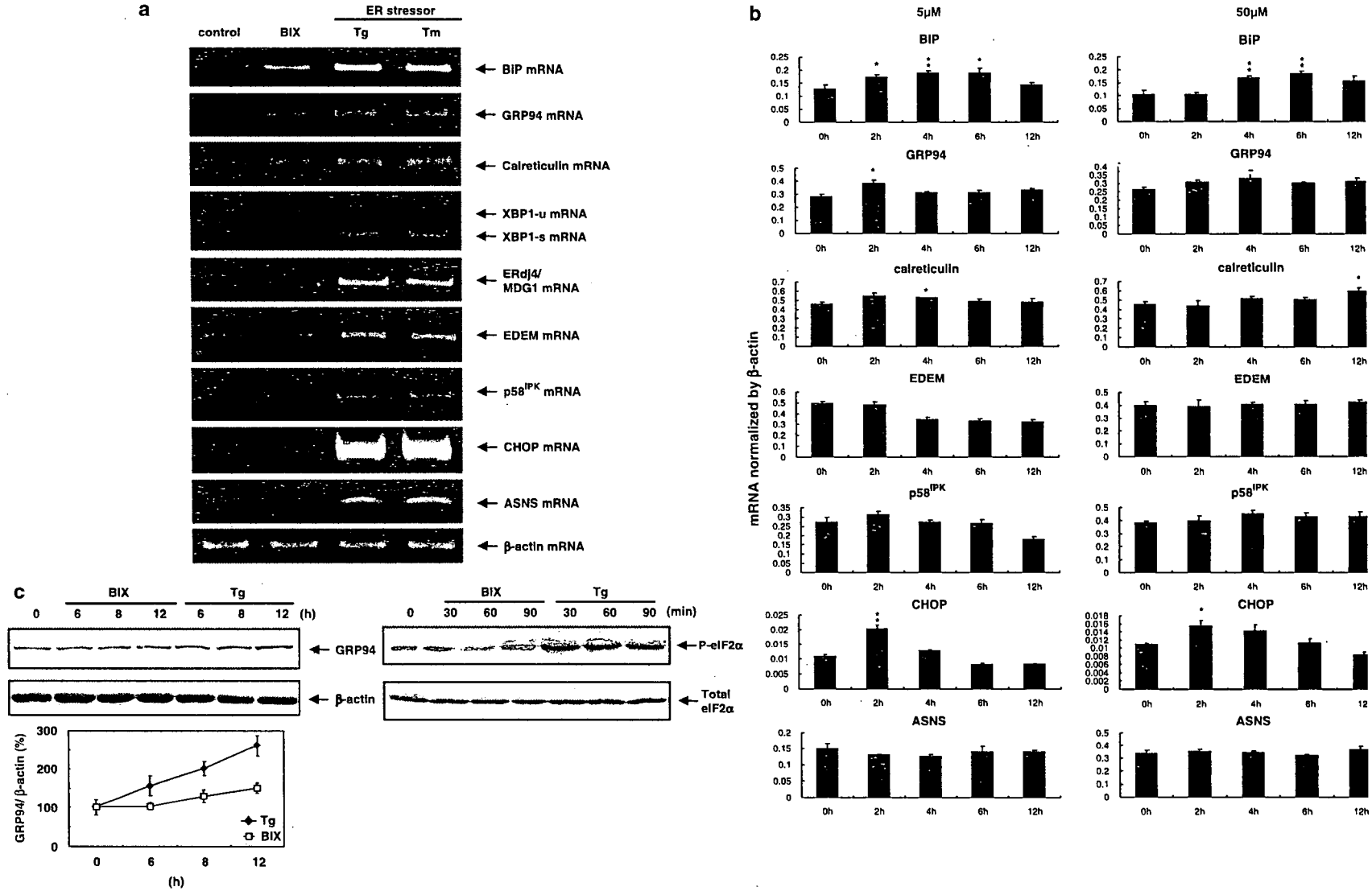

Figure 2 BIX preferentially induces BiP. (**a**) Semiquantitative RT-PCR analysis shows that a 6 h treatment of cells with 5 μM BIX induces BiP mRNA but not spliced XBP1 (XBP1-s), ERdj4/MDG1, EDEM, p58^{IPK}, and ASNS mRNAs, which are induced by 1 μM Tg or 1 μg/ml Tm. GRP94, calreticulin, CHOP are slightly induced by BIX. (**b**) Time-course analyses by real-time PCR show that 5 μM BIX significantly induces BiP from 2 to 6 h after BIX administration and transiently induces GRP94, calreticulin, and CHOP. The mRNAs of EDEM, p58^{IPK}, and ASNS are not changed from 2 to 12 h. A 50 μM portion of BIX also induces BiP from 4 to 6 h and transiently induces calreticulin and CHOP. Even 50 μM BIX does not induce EDEM, p58^{IPK}, and ASNS. Values are means ± S.E. from 3–4 independent experiments. Significant differences are based on the values at 0 h, $^{*}P<0.05$, $^{**}P<0.01$. (**c**) Immunoblot analysis with quantification shows that 5 μM BIX causes very slight induction of GRP94 protein but does not induce the phosphorylation of eIF2α at any time point, compared with 1 μM Tg. Values are means ± S.D. from three independent experiments

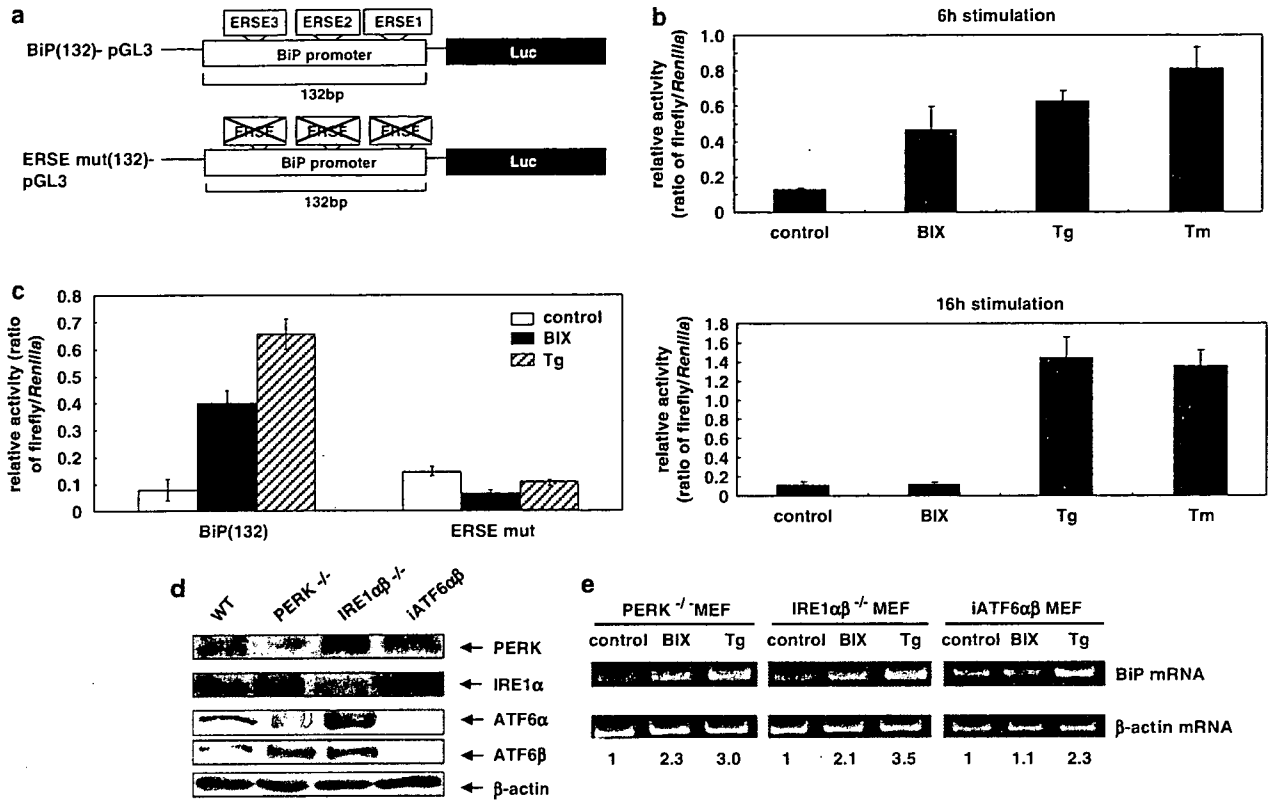

Figure 3 The induction of BiP by BIX is mediated by ERSE and the ATF6 pathway. (a) Schematic representation of the BiP promoter cloned into the pGL3 plasmid (BiP (132)-pGL3) and the ERSE mutant BiP promoter cloned into the pGL3 plasmid (ERSE mut (132)-pGL3). (b) The luciferase activities driven by the BiP promoter are normalized against *Renilla* luciferase activities. The induction of luciferase activity in BiP (132)-pGL3-transfected cells that are treated with 5 μM BIX increased at 6 h after BIX treatment and reversed to basal levels by 16 h. Induction of luciferase activity in 300 nM Tg- or 0.5 μg/ml Tm-treated cells is sustained until 16 h after BIX treatment. Values are means ± S.D. from five independent experiments. (c) The relative reporter activity in cells transfected with BiP (132)-pGL3 (ratio of firefly/*Renilla*) at 6 h after treatment in cells treated with BIX (5 μM) are increased ~4-fold, whereas that in cells transfected with ERSE mut (132)-pGL3 are not increased. Values are means ± S.D. from five independent experiments. Tg (300 nM) also increases reporter activity in cells transfected with BiP (132)-pGL3, but not in cells transfected with mut (132)-pGL3. (d) Immunoblot analyses of PERK$^{-/-}$ MEFs, IRE1$\alpha\beta^{-/-}$ MEFs, and iATF6$\alpha\beta$ (knockdown) MEFs with anti-PERK, anti-IRE1 and anti-ATF6α/β antibodies prove the deficiency of those genes. (e) Semiquantitative RT-PCR analysis shows that BiP mRNA is induced at 6 h after treatment with BIX (50 μM) in PERK$^{-/-}$ MEFs and IRE1$\alpha\beta^{-/-}$ MEFs, but not in iATF6$\alpha\beta$ (knockdown) MEFs. Tg induces BiP mRNA in all three MEFs. Numeric values below the panels indicate the induction ratio of BiP mRNA adjusted to the level of β-actin mRNA with reference to non-treated control sample as one

(Figure 3e). These results indicate that the induction of BiP by BIX is not mediated via the PERK or IRE1 pathways. The data showing that eIF2α is not phosphorylated by BIX (Figure 2c), and that XBP1 is not processed by BIX (Figure 2a), support this conclusion. By contrast, BiP was not induced by BIX in ATF6$\alpha\beta$ double-knockdown MEFs (Figure 3e), suggesting that BIX treatment mediates the induction of BiP via the ATF6 pathway. These results were also obtained by northern blot analysis (data not shown). The data showing that BIX induced GRP94, calreticulin, and CHOP, and that ERdj4/MDG1, EDEM, p58^{IPK} and ASNS were not induced by BIX (Figure 2a, b), also suggested that the effect of BIX is mediated by the ATF6 pathway. This is because the inductions of GRP94, calreticulin, and CHOP are known to be dependent on the activation of ATF6; inductions of ERdj4/MDG1, EDEM, p58^{IPK} are known to be mediated by IRE1 and that of ASNS by PERK. Next, we tried to detect the cleavage of ATF6 in cells treated with BIX, but we have not yet detected cleaved N-terminal fragments of endogenous ATF6 using the antibody described in this study (data not shown).

BIX protects SK-N-SH cells from ER stress-induced apoptosis. BiP functions as a cytoprotective protein in stressed cells.[14–16] As BIX activates BiP expression, BIX might protect cells from ER stress. To investigate whether BIX has the ability to prevent apoptosis induced by ER stress, SK-N-SH cells were pretreated for 12 h with 0 or 5 μM BIX, which was then replaced with fresh medium containing 0.5 μg/ml Tm. Phase-contrast images (Figure 4a–d) and fluorescence micrographs (Figure 4e–h) of Hoechst staining show that apoptotic cell death was observed within 36 h of Tm treatment (Figure 4d, h), and that the number of dead cells had increased significantly (Figure 4i). By contrast, cell death was significantly inhibited by pretreatment with BIX (Figure 4c, g, i). We also found that treatment of cells with BIX only for 36 h caused no changes in cells (Figure 4b, f). Next, we looked at the activation of caspases 4 and 3/7 after ER stress. Caspase 4 was reported to be activated in response to ER stress in human cells.[5] Immunoblot analysis showed that pretreatment of cells with BIX attenuated the cleavage of caspase 4 (Figure 4j). Moreover, we analyzed

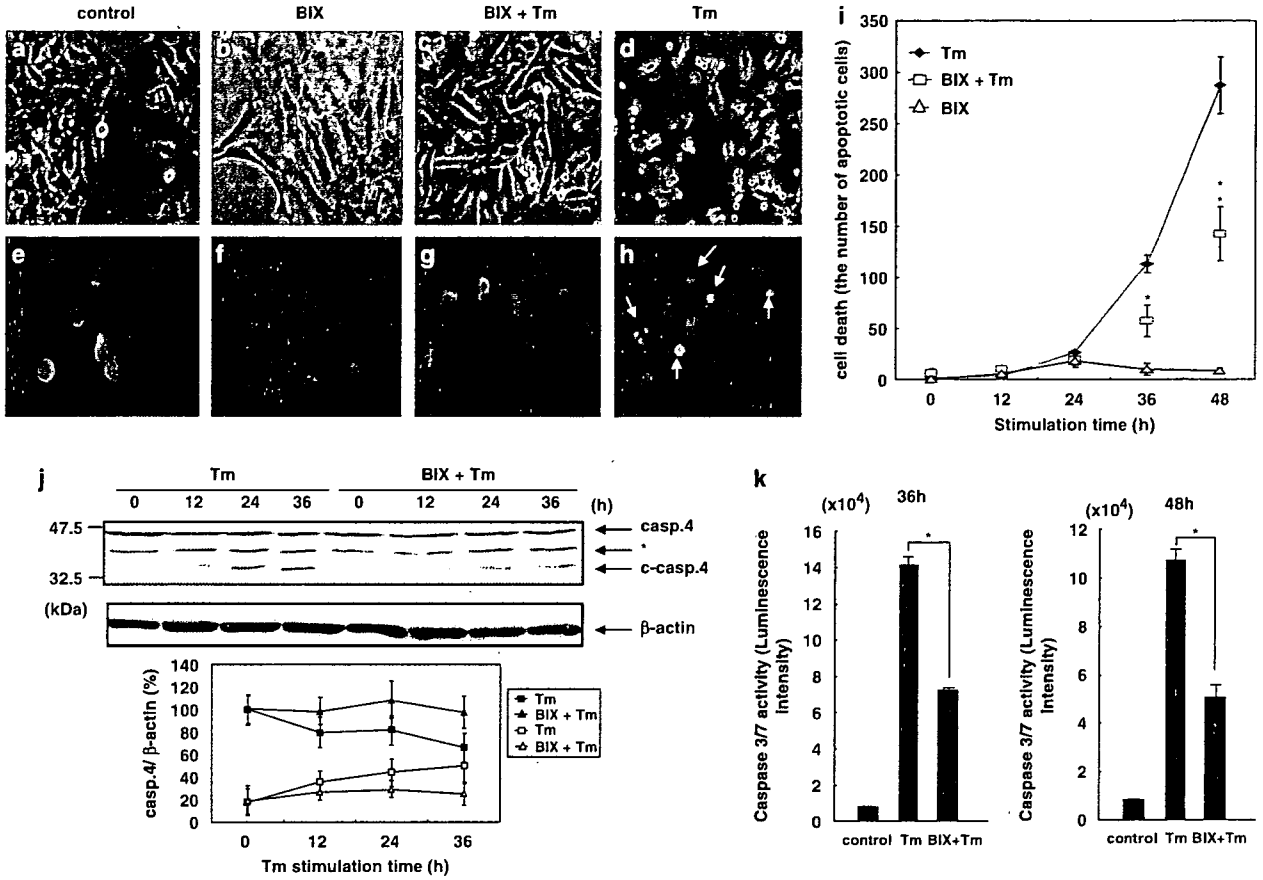

Figure 4 BIX protects SK-N-SH cells from ER stress-induced apoptosis. SK-N-SH cells are pretreated with vehicle (control: **a**, **e**; Tm: **d**, **h**) or with 5 μM BIX (BIX: **b**, **f**; BIX + Tm: **c**, **g**) for 12 h, and then the whole medium is replaced with fresh medium (control, BIX) or medium supplemented with 0.5 μg/ml Tm (BIX + Tm, Tm). Phase-contrast images (**a–d**) and fluorescence micrographs of Hoechst staining (**e–h**) at 36 h after Tm stimulation show that pretreatment of cells with BIX reduces the number of Tm-induced apoptotic cells. Arrows show apoptotic cells (**h**). (**i**) The number of dead cells (apoptotic cells) after Tm treatment increases from 0 to 48 h. Pretreatment of cells with BIX significantly reduces the amount of cell death compared with cells treated with Tm only ($^*P<0.05$, $^{**}P<0.01$). BIX alone does not cause remarkable cell death. A total of 500 cells are counted at each time point. Values are means ± S.D. from five independent experiments. (**j**) Immunoblot of caspase 4 shows that Tm causes cleavage of caspase 4 (c-Casp.4) in a time-dependent manner and that pretreatment of cells with BIX attenuates this cleavage with no change in the level of β-actin. Asterisk indicates nonspecific bands. The lower panel shows quantitative analyses of full-length and cleaved caspase 4. Filled square and triangle indicate full-length caspase 4; open square and triangle indicate cleaved caspase 4. Values are means ± S.D. from three independent experiments. (**k**) The caspases 3 and 7 activities in Tm-treated cells are increased. BIX reduces this caspase activity to almost half value of the Tm-treated levels. Values are means ± S.D. from three independent experiments; $^*P<0.01$

the activities of caspases 3 and 7. The activities of caspases 3 and 7 in Tm-treated cells were extremely high. By contrast, BIX reduced the activities of caspases 3 and 7 to half of those in cells treated with Tm only (Figure 4k). Taken together, these findings suggest that pretreatment of cells with BIX inhibits cell death induced by ER stress involving inhibited activation of caspases 3/7 and 4.

BIX administration reduces the insults due to cerebral infarction. Because it has been shown that cerebral ischemia causes ER stress,[20] we performed occlusions of the middle cerebral arteries (MCAs) of mice to confirm whether the protective effects of BIX *in vitro* can be utilized *in vivo*. Immunoblot analysis of extracts from the cerebral hemisphere showed that 20 μg (2 μl) of BIX (administered intracerebroventricularly) significantly increased the level of BiP protein 24 h after administration, confirming that administration of BIX induces BiP protein *in vivo* (Figure 5a). Real-time PCR analysis of the expression of ER stress response-related genes showed that 20 μg BIX significantly induced BiP at 6 h after administration (Figure 5b). The levels of GRP94, calreticulin, and CHOP mRNA also increased; however, those of EDEM, p58^{IPK}, and ASNS did not change (Figure 5b), consistent with the results of *in vitro* study (Figure 2b). Animals treated with BIX showed no behavioral changes, except for the neurological deficits induced by ischemia. Neurological evaluation at 24 h after MCA occlusion showed that most of the vehicle-administered (control) mice presented with moderate symptoms; for example, circling to the contralateral side (Figure 5c). By contrast, most BIX-administered (5 or 20 μg) mice presented with milder symptoms; for example, extending the right forepaw (Figure 5c).

Twenty-four hours after occlusion, 2,3,5-triphenyltetrazolium chloride (TTC) staining showed that the mice had developed infarcts affecting the ipsilateral cortex and striatum

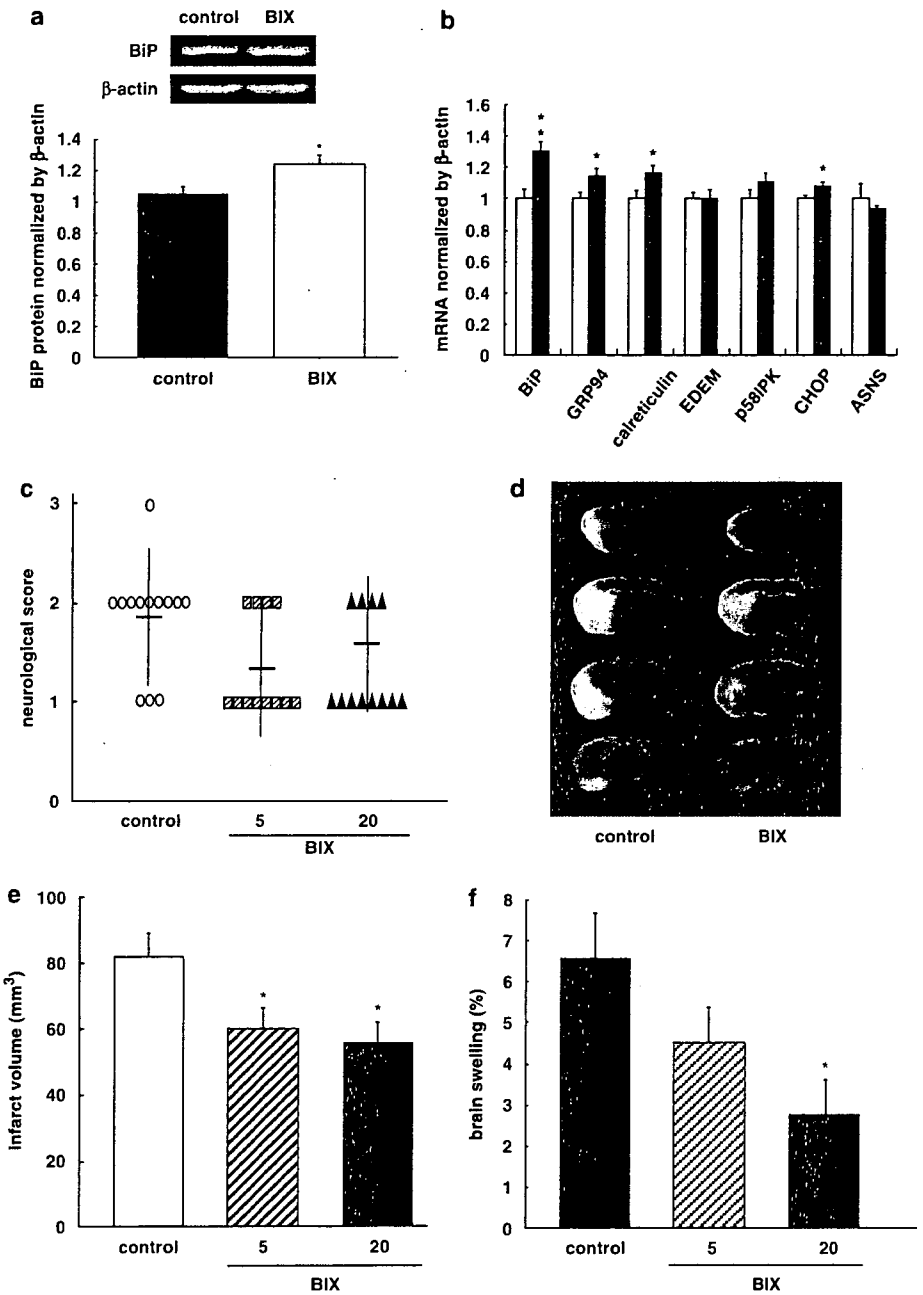

Figure 5 BIX administration reduces the extent of cerebral infarction after MCA occlusion. (**a**) It is confirmed that intracerebroventricular administration of BIX raises the level of BiP protein in mouse brains. Immunoblot analysis of BiP and β-actin protein in BIX-administered (20 μg/2 μl) brains shows that the level of BiP protein is significantly increased at 24 h after BIX administration compared with vehicle-treated brains. The inset is the representative immunoblot detected by luminescence of ECL. Densitometric scanning of BiP bands normalized to β-actin was performed. Data are represented as means ± S.E. from four independent experiments; $^*P<0.05$. (**b**) The real-time PCR shows that the level of BiP (in arbitrary units) in the BIX-administered (20 μg/2 μl) hemisphere is increased significantly at 6 h after administration. The levels of GRP94, calreticulin, and CHOP mRNA are increased by BIX; the levels of EDEM, p58^{IPK}, and ASNS do not change. The black bar is the BIX-administered (20 μg/2 μl) hemisphere; the white bar is the vehicle-administered hemisphere. Values are means ± S.E. from 3–4 independent experiments; $^*P<0.05$, $^{**}P<0.01$. (**c**) Neurological deficits at 24 h after occlusion of the MCA are scored using the following scale: 0 = no observable neurological deficits (normal); 1 = failure to extend the right forepaw (mild); 2 = circling to the contralateral side (moderate); 3 = loss of walking or righting reflex (severe). BIX administration (5 or 20 μg) improves neurological deficits induced by MCA occlusion. Values are means (horizontal bold bar) ± S.D. (**d**) Representative images of TTC staining at 24 h after MCA occlusion. Note that the infarct area (white or pink) in BIX-administered brains is smaller than that in brains treated with vehicle. (**e**) Quantitative analysis of infarct volumes measured by TTC staining. Values are means ± S.E. from 12 or 13 independent experiments; $^*P<0.05$. (**f**) BIX administration (5 or 20 μg) reduces brain swelling induced by MCA occlusion. Values are means ± S.E. from 12 or 13 independent experiments; $^*P<0.05$

(Figure 5d). The core of infarction was observed as a white area and the penumbra was pink. The infarction area (core + penumbra) observed in BIX-treated brains was smaller than that in vehicle-treated brains (Figure 5d). Quantitation of TTC staining showed that administration of 5 or 20 μg of BIX significantly reduced the infarction area (Figure 5e). Furthermore, measurement of brain swelling also showed that administration of 20 μg of BIX significantly reduced brain swelling after 24 h of ischemia (Figure 5f).

BIX administration reduces apoptosis induced in the penumbra by MCA occlusion. Detailed observation of TTC-stained ischemic brains indicated that the reduction in the area of infarction in BIX-treated brains was predominantly due to a reduction in the area of the penumbra rather than the core. Therefore, we examined the penumbra of BIX-treated brain for evidence of apoptosis. Terminal deoxynucleotidyl transferase-mediated dUTP–biotin nick end labeling (TUNEL) staining of ischemic brains without BIX treatment revealed an increased number of TUNEL-positive cells in the ipsilateral core and penumbra compared with the contralateral side (Figure 6a). By contrast, the number of TUNEL-positive cells was significantly reduced in the ipsilateral penumbra of BIX-treated brains compared with that of vehicle-treated brains (Figure 6a, b). Immunohistochemistry for caspase 3 in the penumbrae of BIX- and vehicle-treated brains showed that BIX reduced the number of apoptotic cells at 24 h after MCA occlusion (Figure 6c, d). CHOP plays a role in apoptotic cell death by ER stress.[21] Moreover, it is well-known that CHOP is induced after ischemic insults.[22] Therefore, we examined the effects of BIX treatment on the induction of CHOP mRNA after ischemia. *In situ* hybridization analysis showed that CHOP mRNA was significantly induced in the penumbra of MCA-occluded mice, whereas pretreatment of mice with BIX resulted in a marked reduction in the level of CHOP mRNA expression (Figure 6e, f). Although BIX induced CHOP (Figure 5b), the extent of this induction was very weak compared with the expression induced by ischemia (Figure 6e, f). The results of TUNEL staining and *in situ* hybridization for CHOP indicate that BIX suppresses the ER stress-mediated apoptotic cell death induced in the penumbra after ischemia.

Discussion

If a BiP inducer is just an ER stressor such as Tg or Tm, its application as a therapeutic strategy is unlikely to be realized because it may activate several pathways of the UPR, including ER stress-induced apoptotic pathways. The present studies in knockout or knockdown MEFs deficient in ER stress sensors showed that the ATF6 pathway is necessary for BIX to induce BiP. This is consistent with the evidence that BIX preferentially induced BiP with slight inductions of GRP94, calreticulin, and CHOP mediated by the ATF6 pathway, and that BIX does not affect the pathway downstream of IRE1 or the translational control branch downstream of PERK. Moreover, for the apoptotic branches of ER stress, the transient induction of CHOP by BIX was very weak compared with the severe induction observed in ER stress, and caspase 4 was not activated by BIX. The differences among inductions between BiP and the other genes of the ATF6 pathway by BIX suggested that elements other than ERSEs may be involved in the induction of BiP by BIX.

The present data from *in vitro* studies showed that BIX suppresses the cleavage of caspase 4, a member of one of the apoptotic pathways mediated by ER stress. Because it was reported that PERK is activated after cerebral ischemia[10] and that XBP1 mRNA splicing is detected after transient cerebral ischemia,[11] it would appear that cerebral ischemia causes ER stress. Thus, to examine the antiapoptotic effect of BIX *in vivo*, we used MCA-occluded mice. Intracerebroventricular pretreatment of mice with BIX reduced the area of infarction in the brain, especially the area of the penumbra. BIX pretreatment also reduced the severity of neurological deficits caused by focal cerebral ischemia. In the penumbrae of BIX-treated brains, the induction of CHOP, an apoptotic molecule induced by ER stress, was suppressed, suggesting that BIX reduces cell death by preventing ER stress-induced apoptosis. As the infarct volumes, brain swelling, and neurological scores following 5 and 20 μg treatments were similar, 5 μg of BIX might be sufficient to protect against ischemia. This is the first report demonstrating the *in vivo* success of a therapeutic manipulation to inhibit apoptosis mediated by ER stress, indicting that BIX might be a potential therapeutic for neuroprotection after cerebral infarction.

The induction of BiP by BIX was transient, peaking at 4 h after treatment, but the levels of BiP protein continued to increase until 12 h. The reporter assay using the 132 bp BiP-pGL3 plasmid also showed that the effect of BIX on the induction of BiP was transient and weaker than the effect of ER stressors, such as Tg or Tm. Even a high dosage of BIX (50 μM) did not induce genes mediated by non-ATF6 pathways. These results imply that the mechanism of BiP induction utilized by BIX may be different from those used by these ER stressors. It was reported that the activation of transducers of ER stress is caused by dissociation of BiP from their luminal domains.[23] It may be assumed that artificial induction of BiP disturbs the activation of transducers of ER stress, because abundant BiP remains bound to these transducers preventing their activation. However, the effect of BIX peaked at 4 h and remained at that level until 6 h after treatment; after this point, there was a subsequent reduction in level. Therefore, the production of BiP induced by BIX may not disturb this dissociation.

An earlier study showed that a selective inhibitor of eIF2α dephosphorylation protects cells from ER stress[12] and that the development of novel chemical compounds for diseases related to ER stress is underway. It is possible that BIX, which has effects *in vivo*, could have therapeutic applications in the treatment of diseases involving ER stress. We propose that BiP activators, such as BIX, will be effective agents against ER stress. However, further studies will be required to investigate the pharmacology of BIX, including its possible side effects, before BiP activators can be used in clinical practice.

Materials and Methods

Cell culture. SK-N-SH neuroblastoma cells were grown in α-modified Eagle's medium supplemented with 10% fetal bovine serum. MEFs derived from IRE1$^{-/-}$ embryos or PERK$^{-/-}$ embryos were cultured in Dulbecco's modified Eagle's

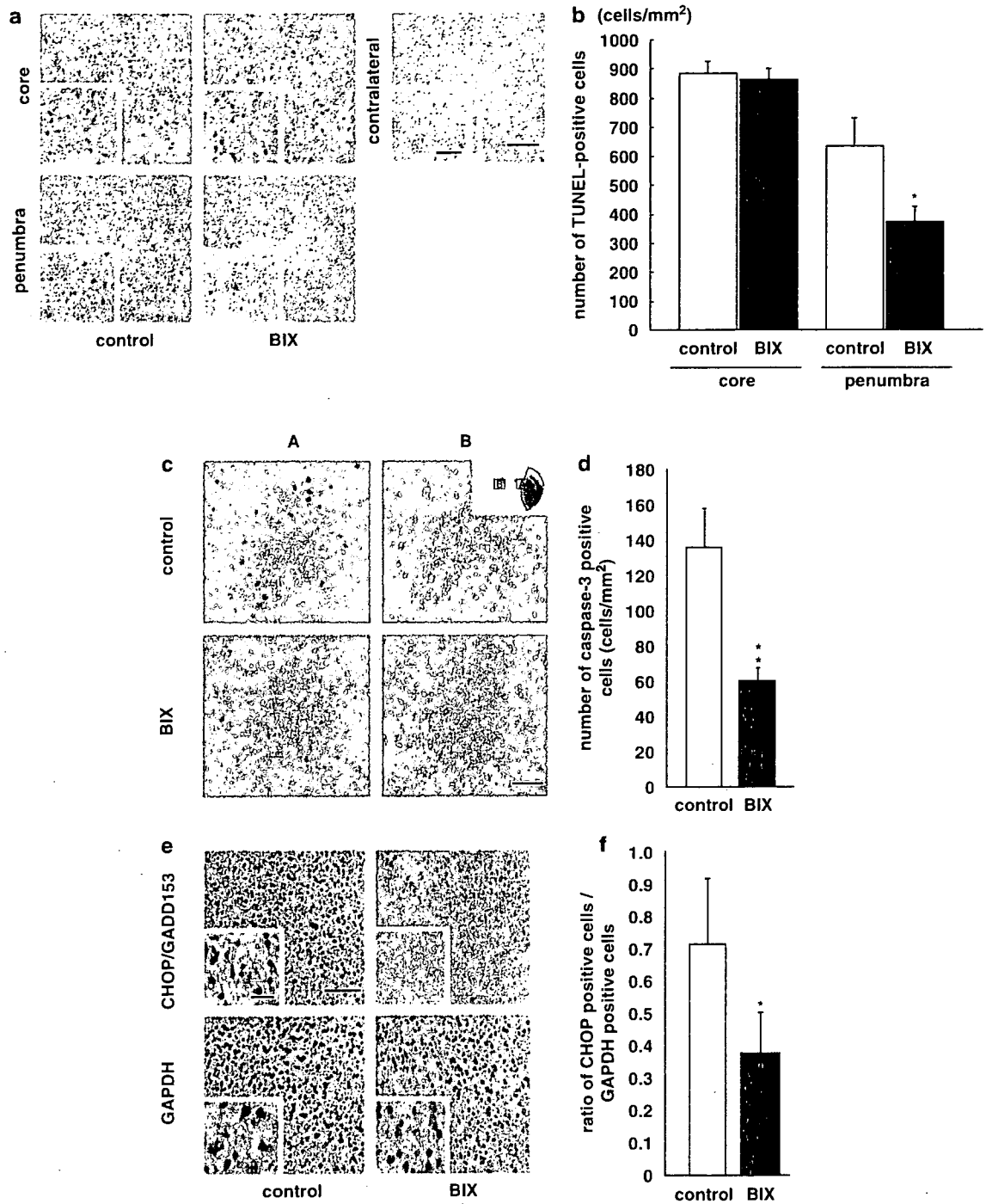

Figure 6 A 20 μg portion of BIX administration reduces ER stress-induced apoptosis induced in the penumbra by MCA occlusion. (a) Representative images of TUNEL staining in the core, penumbra, or contralateral side to the infarction at 24 h. Insets are higher magnification images. BIX administration reduces the number of TUNEL-positive cells induced in the penumbra by MCA occlusion. Scale bar for higher magnification panels, 10 μm; lower magnification panels, 100 μm. (b) Cell-counting analysis shows that BIX significantly reduced the number of TUNEL-positive cells in the penumbra. Values are means ± S.D. from 9 or 10 independent experiments; $^{*}P<0.05$. (c) Representative image showing immunohistochemical staining for caspase 3 in the penumbra area (**A**) and contralateral area (**B**) in a BIX-treated mouse and vehicle-treated mouse at 24 h after treatment. Scale bar, 50 μm. (d) Quantitative analysis of caspase 3-positive cells. Values shown are the number of caspase 3-positive cells/mm^2. Values are means ± S.D. from five independent experiments; $^{**}P<0.01$. (e) Representative images of *in situ* hybridization for CHOP, an apoptotic molecule induced in penumbra by ER stress at 24 h. Insets are higher magnification images. Scale bar for higher magnification panels, 10 μm; lower magnification panels, 100 μm. (f) Quantitative analysis of CHOP-positive cells. Values shown are the ratios of CHOP-/GAPDH-positive cells. Values are means ± S.D. from five independent experiments; $^{*}P<0.05$

medium supplemented with 10% fetal bovine serum. MEFs in which both ATF6α and ATF6β (iATF6$\alpha\beta$MEF) had been knocked down were also maintained in the Dulbecco's modified Eagle's medium. PERK$^{-/-}$ MEFs, IRE1$^{-/-}$ MEFs, and iATF6$\alpha\beta$MEFs were kindly provided by Drs. David Ron (New York University, NY, USA), Dr. Fumihiko Urano (University of Massachusetts Medical School, MA, USA), and Laurie H Glimcher (Harvard School of Public Health, MA, USA), respectively.

Reagents. Cells were treated with Tm or Tg to induce ER stress conditions. Tm was purchased from Sigma (St. Louis, MO, USA). Tg was purchased from Alomone Labs Ltd (Jerusalem, Israel). Hoechst staining was performed according to the manufacturer's instructions.

Plasmids. A pGL3-BiP promoter (132)-Luc reporter plasmid (BiP (132)-pGL3) and an ERSE mutant BiP promoter-Luc reporter plasmid (ERSE mut (132)-pGL3) were provided by Dr. K Mori (Kyoto University, Kyoto, Japan).

Transfection and reporter assays. SK-N-SH cells were grown to 80% confluence and then transfected using Lipofectamine 2000 reagent, according to the manufacturer's instructions (Invitrogen, Carlsbad, CA, USA). Cells were transfected with a reporter plasmid (0.2 μg) carrying the firefly luciferase gene under the control of the BiP promoter, and a reference plasmid pRL-SV40 (0.02 μg) carrying the *Renilla* luciferase gene under the control of the SV40 enhancer and promoter (Promega, Madison, WI, USA). At 12 h after transfection, cells were treated with library compounds to screen for compounds that induce BiP. Firefly and *Renilla* luciferase activities were measured in 10 μl of cell lysate using a Dual-Luciferase Reporter Assay System (Promega) and a luminometer (Berthold Technologies, Bad Wildbad, Germany). Relative luciferase activity was defined as the ratio of firefly luciferase activity to *Renilla* luciferase activity. Values were averaged from quadruplicate determinations. Using these BiP reporter cells, HTS was performed on a compound library consisting of approximately 10 000 compounds. The molecules were synthesized based on the structures of 10 lead compounds that had high activity in HTS. Among the synthesized molecules, we chose a small molecule that had the highest activity, naming it BIX. To confirm the induction of BiP by this compound, 5 μM BIX, 300 nM Tg or 0.5 μg/ml Tm were added to cell and the luciferase assay was performed as described; luciferase activities were measured in three independent experiments.

RNA isolation and semiquantitative RT-PCR analysis. SK-N-SH cells or MEFs were washed with phosphate-buffered saline (PBS) and then collected by centrifugation. Total RNA was isolated from cells using an RNeasy kit (Qiagen, Tokyo, Japan) according to the manufacturer's protocol. Total RNA was isolated from frozen brains using the acid guanidine–phenol–chloroform RNA extraction method provided as ISOGEN (Nippon Gene, Toyama, Japan), and purified using an RNeasy Mini kit (Qiagen). RNA concentrations were determined spectrophotometrically at 260 nm. First-strand cDNA was synthesized in a 20-μl reaction volume using a random primer (Takara, Shiga, Japan) and Moloney murine leukemia virus reverse transcriptase (Invitrogen). PCR was performed in a total volume of 30 μl containing 0.8 μM of each primer, 0.2 mM dNTPs, 3 U *Taq* DNA polymerase (Promega), 2.5 mM $MgCl_2$, and 1 × PCR buffer. The amplification conditions for semiquantitative RT-PCR analysis were as follows: an initial denaturation step of 95°C for 5 min, 22 cycles of 95°C for 1 min, 55°C for 1 min, and 72°C for 1 min, and a final extension step of 72°C for 7 min. The numbers of amplification cycles for detection of BiP and β-actin were 18 and 15, respectively. The primers used for amplification were as follows: BiP: 5′-GTTTGCTGAGG AAGACAAAAAGCTC-3′ and 5′-CACTTCCATAGAGTTTGCTGATAATTG-3′; XBP1: 5′-CAGCGCTTGGGGATGGATGC-3′ and 5′-CCATGGGGAGATGTTCTG GA-3′; CHOP: 5′-GGAGCTGGAAGCCTGGTATGAGG-3′ and 5′-TCCCTGGTCA GGCGCTCGATTTCC-3′; GRP94: 5′- CTCACCATTTGGATCCTGTGTG-3′ and 5′-CACATGACAAGATTTTACATCAAGA-3′; calreticulin: 5′-GCCAAGGACGAGCT GTAGAGAG-3′ and 5′-GGTGAGGGCTGAAGGAGAATC-3′; ERdj4/MDG1: 5′-TCTAGAATGGCTACTCCCCAGTCAATTTTC-3′ and 5′-TCTAGACTACTGTCCT GAACAGTCAGTG-3′; EDEM: 5′-TGGGTTGGAAAGCAGAGTGGC-3′ and 5′-TCCATTCCTACATGGAGGTAG-3′; p58^{IPK} 5′-GAGGTTTGTGTTTGGGATGCAG-3′ and 5′-GCTCTTCAGCTGACTCAATCAG-3′; ASNS: 5′-AGGTTGATGATGCAATG ATGG-3′ and 5′-TCCCCTATCTACCCACAGTCC-3′; β-actin: 5′-TCCTCCCTGGA GAAGAGCTAC-3′ and 5′-TCCTGCTTGCTGATCCACAT-3′. PCR products were resolved by electrophoresis through 4.8% (w/v) polyacrylamide gels. The density of each band was quantified using the Scion Image Program (Scion Corporation, Frederick, MD, USA).

Northern blot analysis. Total RNA (10 μg/lane) was resolved by electrophoresis through 1.0% agarose/formaldehyde gels and transferred onto Immobilon-NY + membranes (Millipore, Bedford, MA, USA). Filters were hybridized with ^{32}P-labeled cDNA probes generated from the BiP cDNA by the Random Primer DNA labeling kit (Takara). After washing in 2 × SSC/0.1% SDS and 0.1 × SSC/0.1% SDS, filters were exposed onto IP plates (Fuji Film, Tokyo, Japan) and analyzed using a BAS1800 system (Fuji Film).

Real-time PCR. TaqMan real-time PCR was performed as described previously.[24] Single-stranded cDNA was synthesized from total RNA using a High-Capacity cDNA Archive Kit (Applied Biosystems, Foster City, CA, USA). Quantitative real-time PCR was performed using an ABI PRISM™ 7900HT Sequence Detection System (Applied Biosystems) with a TaqMan Universal PCR Master Mix (Applied Biosystems) according to the manufacturer's protocol. The expressions of mRNAs were measured by real-time PCR using the Applied Biosystems Assays-on-Demand™ Gene Expression Product. The thermal cycler conditions were as follows: 2 min at 50°C and then 10 min at 95°C, followed by two-step PCR for 50 cycles consisting of 95°C for 15 s followed by 60°C for 1 min. For each PCR, we checked the slope value, R^2 value, and linear range of a standard curve of serial dilutions. All reactions were performed in duplicate. The results are expressed relative to the β-actin, internal control.

Immunoblot analysis. Cells were washed with PBS, harvested and lysed in Nonidet P-40 lysis buffer (1% Nonidet P-40, 20 mM HEPES (pH 7.6), 100 mM NaCl, 3 mM $MgCl_2$, 5 mM dithiothreitol, and 0.1% protease inhibitor cocktail (Sigma)). Lysates were then sonicated on ice three times for 5 s and centrifuged at 15 000 r.p.m. for 5 min. Supernatants were retained and boiled for 5 min in SDS sample buffer. Equal amounts of protein were subjected to 10–15% SDS-PAGE, transferred to PVDF membranes, and immunoblotted with each primary antibody. Membranes were washed with TBS/Tween-20, and then incubated with an alkaline phosphatase-conjugated secondary antibody (Sigma). The corresponding bands were detected using ECL Plus Western Blotting Detection System (GE Healthcare UK Ltd, Buckinghamshire, England). The density of each band was quantified using the Scion Image Program (Scion Corporation). As primary antibodies, anti-PERK antibody was provided by Dr. David Ron (New York University) and anti-IRE1α antibody was provided by Dr. Fumihiko Urano (University of Massachusetts Medical School). Anti-KDEL (Stressgen, Victoria, BC, Canada), anti-total eIF2α (Cell signaling Technology, Beverly, MA, USA), anti-eIF2α (phosphospecific) (Stressgen), anti-ATF6α (Santa Cruz Biotechnology, Santa Cruz, CA, USA), anti-ATF6β (Santa Cruz Biotechnology), anti-TX (MBL Co. Ltd, Nagoya, Japan), and anti-actin (Chemicon, Temecula, CA, USA) antibodies were purchased commercially. Anti-KDEL antibody detected BiP and GRP94. Anti-TX antibody detected caspase 4 protein.

Caspase activity. SK-N-SH cells were seeded into 96-well culture plates (1.0×10^4 cells/well). Cells were cultured under standard conditions for 12 h, and then treated with 5 μM BIX or vehicle for another 12 h. After BIX or vehicle treatment, the whole medium was replaced with fresh medium containing 0.5 μg/ml Tm and cells were incubated for additional 36 or 48 h. After incubation, caspase-3 and -7 activity was measured using a caspase-Glo 3/7 Assay kit (Promega), according to the manufacturer's instructions. Luminescent signals were measured using a luminometer (Berthold Technologies). The measurement of caspases 3 and 7 activities was conducted in three independent experiments.

Cell death assay. SK-N-SH cells were pretreated with 5 μM BIX or vehicle for 12 h, after which the whole medium was replaced with fresh medium containing 0.5 μg/ml Tm, in which cell were cultured for the indicated times. Cells were fixed with 4% paraformaldehyde for 30 min at 4°C, washed with PBS for 5 min, and then stained with 100 μM Hoechst 33258 (Wako Pure Chemical Co., Tokyo, Japan) in PBS for 20 min. A total of 500 cells were counted randomly and apoptotic cells were determined by fluorescence microscopy.

Focal cerebral ischemia model in mice. Male adult ddY mice weighing 24–34 g (Japan SLC) were used in experiments, and were housed under diurnal lighting conditions. Anesthesia was induced by 2.0% isoflurane, then maintained using 1% isoflurane in 70% N_2O and 30% O_2 using an animal general anesthesia machine (Soft Lander, Sin-ei Industry Co. Ltd, Saitama, Japan). Body temperature was maintained between 37.0 and 37.5°C with the aid of a heating pad and heating lamp. A filament occlusion of the left MCA was carried out as previously

described.[25,26] Briefly, the left MCA was occluded with an 8-0 nylon monofilament (Ethicon, Somerville, NJ, USA) coated with a mixture of silicone resin (Xantopren; Bayer Dental, Osaka, Japan). This coated filament was introduced into the internal carotid artery through the common carotid artery up to the origin of the anterior cerebral artery, so as to occlude the MCA and posterior communicating artery. At the same time, the left common carotid artery was occluded by the suture. Permanent ischemia was selected because it produced a reproducible subtotal infarction in our previous studies.[25,26] Twenty-four hours after the occlusion, the forebrain was divided into five coronal 2 mm sections using a mouse brain matrix (RBM-2000C; Activational Systems, Warren, MI, USA). Sections were then stained with 2% TTC. Images of the infarcted areas were recorded using a digital camera (Nikon, COOLPIX4500), quantitated using Image J software (http://rsb.info.nih.gov/ij/download/), and calculated as in a previous report.[26] Brain swelling was calculated according to the following formula: (infarct volume + ipsilateral undamaged volume − contralateral volume) × 100/contralateral volume (%).[25] BIX was dissolved in 10% DMSO and fresh solution was made daily. DMSO (10%) was used as a control. Physiologic parameters were recorded according to our previously described method.[25] In brief, a polyethylene catheter was inserted into the femoral artery to sample arterial blood (30 μl) and measure blood pressure. After the catheter had been inserted into the femoral artery, 2 μl of BIX at 2.5 or 10 μg/μl was intracerebroventricularly administered 30 min before the start of the ischemia, because we do not know the permeability of BIX to the blood brain barrier. Body temperature, arterial blood pressure, pO_2, pCO_2, pH, and plasma glucose were measured 15 min after the start of the ischemia. There were no significant differences in physiological parameters between the vehicle- and BIX-treated groups (data not shown). After 30 min of ischemia, vehicle- and BIX-treated mice exhibited moderate neurological deficits (such as circling, decreased resistance to lateral pushing, decreased locomotor activity, flexion of the right (contralateral to the ischemia) torso and forelimb upon lifting the animal by its tail, and abnormal posture). Animals showing no neurological deficits at 30 min after the occlusion were removed from the study on the grounds that they had not undergone successful occlusion of the MCA. We removed 2 out of 15, 1 out of 13, and 1 out of 13 mice in control, 5 μg BIX-treated, and 20 μg BIX-treated groups, respectively. The present experiments were performed in accordance with the Guidelines for Animal Experiments of Gifu Pharmaceutical University.

Neurological deficits. Mice were tested for neurological deficits at 24 h after MCA occlusion and scored as described previously[25] using the following scale: 0 = no observable neurological deficits (normal); 1 = failure to extend the right forepaw (mild); 2 = circling to the contralateral side (moderate); 3 = loss of walking or righting reflex (severe). The investigator who rated the mice was blinded as to the group to which each mouse belonged.

Immunohistochemistry. At 24 h after MCA occlusion, mice were injected with sodium pentobarbital (nembutal; 50 mg/kg, i.p.), and then perfused through the left ventricle with 4% paraformaldehyde in 0.1 M phosphate buffer (PB; pH 7.4). Brains were removed after 15 min of perfusion fixation at 4°C and immersed in the same fixative solution overnight at 4°C. They were then immersed in 25% sucrose in 0.1 M PB for 24 h, and finally frozen in powdered dry ice. Coronal sections (10 μm) were cut on a cryostat at −20°C and stored at −80°C until use. After rehydration, endogenous peroxidase activity was quenched using 1% hydrogen peroxidase in methanol. Next, brain sections were blocked with 3% BSA in PBS/0.1% Triton X-100 for 1 h, and then incubated overnight at 4°C with primary antibody in the same buffer. Sections were washed and then incubated with biotinylated secondary antibody before being incubated for 30 min at room temperature with avidin–biotin–peroxidase complex, and then developed using diaminobenzidine (DAB) peroxidase substrate. Caspase 3-stained cells were counted in the striatum. The results are expressed as positive cells per 1 mm^2.

TUNEL staining. Apoptosis was detected using the TUNEL method using an *in situ* cell death detection kit, POD (Roche, Penzberg, Germany). TUNEL signals were developed using a DAB peroxidase substrate kit (Vector Labs, Burlingame, CA, USA).

***In situ* hybridization histochemistry.** CHOP and GAPDH cDNAs were subcloned into pGEM-T Easy and pBluescript vectors, respectively. Digoxigenin-labeled cRNA probes were made by *in vitro* transcription in the presence of digoxigenin using subcloned cDNAs for these genes as templates. *In situ* hybridization using digoxigenin-labeled cRNA probes was performed as previously described.[27]

Statistical analysis. Statistical comparisons were made using a one-way ANOVA followed by a Student's *t*-test, Dunnett's test, or the Mann–Whitney *U*-test. STATVIEW version 5.0 (SAS Institute Inc., Cary, NC, USA) was used for statistical analyses. $P < 0.05$ was considered to indicate statistical significance.

Acknowledgements. We thank Dr. David Ron for the PERK$^{-/-}$ MEFs and the anti-PERK antibody, Dr. Fumihiko Urano for the IRE1$^{-/-}$ MEFs and the anti-IRE1α antibody, Dr. Laurie H Glimcher for the iATF6$\alpha\beta$MEFs, and Dr. K Mori for the BiP-pGL3 reporter plasmid. We also thank Ms Mikiko Kubo for her technical assistance. This work was supported by a Grant-in-Aid for Scientific Research (17200026) from the Japan Society for the Promotion of Science and Research on Psychiatric and Neurological Diseases and Mental Health from the Japan Ministry of Health, Labor, and Welfare. This study was supported by the Program for Promotion of Fundamental Studies in Health Sciences of the National Institute of Biomedical Innovation. Funding was also provided by the Japan Society for the Promotion of Science (SK).

1. Zhang K, Kaufman RJ. The unfolded protein response: a stress signaling pathway critical for health and disease. *Neurology* 2006; **66** (Suppl 1): s102–s109.
2. Katayama T, Imaizumi K, Sato N, Miyoshi K, Kudo T, Hitomi J *et al.* Presenilin-1 mutations downregulate the signalling pathway of the unfolded-protein response. *Nat Cell Biol* 1999; **8**: 479–485.
3. Katayama T, Imaizumi K, Honda A, Yoneda T, Kudo T, Takeda M *et al.* Disturbed activation of endoplasmic reticulum stress transducers by familial Alzheimer's disease-linked presenilin 1 mutations. *J Biol Chem* 2001; **276**: 43446–43454.
4. Yasuda Y, Kudo T, Katayama T, Imaizumi K, Yatera M, Okochi M *et al.* FAD-linked presenilin-1 mutants impede translation regulation under ER stress. *Biochem Biophys Res Commun* 2002; **296**: 313–318.
5. Hitomi J, Katayama T, Eguchi Y, Kudo T, Taniguchi M, Koyama Y *et al.* Involvement of caspase-4 in endoplasmic reticulum stress-induced apoptosis and Aβ-induced cell death. *J Cell Biol* 2004; **165**: 347–356.
6. Kitada T, Asakawa S, Hattori N, Matsumine H, Yamamura Y, Minoshima S *et al.* Mutations in the Parkin gene cause autosomal recessive juvenile Parkinsonism. *Nature* 1998; **392**: 605–608.
7. Imai Y, Soda M, Inoue H, Hattori N, Mizuno Y, Takahashi R. An unfolded putative transmembrane polypeptide, which can lead to endoplasmic reticulum stress, is a substrate of Parkin. *Cell* 2001; **105**: 891–902.
8. Nishitoh H, Matsuzawa A, Tobiume K, Saegusa K, Takeda K, Hori S *et al.* ASK1 is essential for endoplasmic reticulum stress-induced neuronal cell death triggered by expanded polyglutamine repeats. *Gene Dev* 2002; **16**: 1345–1355.
9. Bence NF, Sampat RM, Kopito RR. Impairment of the ubiquitin–proteasome system by protein aggregation. *Science* 2001; **292**: 1552–1555.
10. Kumar R, Azam S, Sullivan JM, Owen C, Cavener DR, Zhang P *et al.* Brain ischemia and reperfusion activates the eukaryotic initiation factor 2alpha kinase, PERK. *J Neurochem* 2001; **77**: 1418–1421.
11. Paschen W, Aufenberg C, Hotop S, Mengesdorf T. Transient cerebral ischemia activates processing of xbp1 messenger RNA indicative of endoplasmic reticulum stress. *J Cereb Blood Flow Metab* 2003; **23**: 449–461.
12. Boyce M, Bryant KF, Jousse C, Long K, Harding HP, Scheuner D *et al.* A selective inhibitor of eIF2α dephosphorylation protects cells from ER stress. *Science* 2005; **307**: 935–939.
13. Kim AJ, Shi Y, Austin RC, Werstuck GH. Valproate protects cells from ER stress-induced lipid accumulation and apoptosis by inhibiting glycogen synthase kinase-3. *J Cell Sci* 2005; **118**: 89–99.
14. ZaiFang Y, Luo H, Weiming F, Mattson MP. The endoplasmic reticulum stress-responsive protein GRP78 protects neurons against excitotoxicity and apotosis: suppression of oxidative stress and stabilization of calcium homeostasis. *Exp Neurol* 1999; **155**: 302–314.
15. Rao RV, Peel A, Logvinova A, del Rio G, Hermel E, Yokota T *et al.* Coupling endoplasmic reticulum stress to the cell death program: role of the ER chaperone GRP78. *FEBS Lett* 2002; **514**: 122–128.
16. Reddy RK, Mao C, Baumeister P, Austin RC, Kaufman RJ, Lee AS. Endoplasmic reticulum chaperone protein GRP78 protects cells from apoptosis induced by topoisomerase inhibitors: role of ATP binding site in suppression of caspase-7 activation. *J Biol Chem* 2003; **278**: 20915–20924.
17. Gomer C, Ferrario A, Rucker N, Wong S, Lee AS. Glucose regulated protein induction and cellular resistance to oxidative stress mediated by porphyrin photosensitization. *Cancer Res* 1991; **51**: 6574–6579.
18. Li LJ, Li X, Ferrario A, Rucker N, Liu ES, Wong S *et al.* Establishment of a Chinese hamster ovary cell line that expresses grp78 antisense transcripts and suppresses A23187 induction of both GRP78 and GRP94. *J Cell Physiol* 1992; **153**: 575–582.

19. Sugawara S, Takeda K, Lee A, Dennert G. Suppression of stress protein GRP78 induction in tumor B/C10ME eliminates resistance to cell mediated cytotoxicity. *Cancer Res* 1993; 53: 6001–6005.
20. DeGracia DJ, Montie HL. Cerebral ischemia and the unfolded protein response. *J Neurochem* 2004; 91: 1–8.
21. Kaufman RJ. Orchestrating the unfolded protein response in health and disease. *J Clin Invest* 2002; 110: 1389–1398.
22. Tajiri S, Oyadomari S, Yano S, Morioka M, Gotoh T, Hamada JI *et al.* Ischemia-induced neuronal cell death is mediated by the endoplasmic reticulum stress pathway involving CHOP. *Cell Death Differ* 2004; 11: 403–415.
23. Bertolotti A, Zhang Y, Hendershot LM, Harding HP, Ron D. Dynamic interaction of BiP and ER stress transducers in the unfolded-protein. *Nat Cell Biol* 2000; 2: 326–332.
24. Chen D, Padiernos E, Ding F, Lossos IS, Lopez CD. Apoptosis-stimulating protein of p53-2 (ASPP2/^{53BP2L}) is an E2F target gene. *Cell Death Differ* 2005; 12: 358–368.
25. Hara H, Huang PL, Panahian N, Fishman MC, Moskowitz MA. Reduced brain edema and infarction volume in mice lacking the neuronal isoform of nitric oxide synthase after transient MCA occlusion. *J Cereb Blood Flow Metab* 1996; 16: 605–611.
26. Hara H, Friedlander RM, Gagliardini V, Ayata C, Fink K, Huang Z *et al.* Inhibition of interleukin 1β converting enzyme family proteases reduces ischemic and excitotoxic neuronal damage. *Proc Natl Acad Sci USA* 1997; 94: 2007–2012.
27. Honma Y, Kanazawa K, Mori T, Tanno Y, Tojo M, Kiyosawa H *et al.* Identification of a novel gene, OASIS, which encodes for a putative CREB/ATF family transcription factor in the long-term cultured astrocytes and gliotic tissue. *Brain Res Mol Brain Res* 1999; 69: 93–103.

The FASEB Journal • Research Communication

A family of membrane proteins associated with presenilin expression and γ-secretase function

Wataru Araki,*[,1] Noriko Takahashi-Sasaki,[†] De-Hua Chui,[‡] Shinya Saito,* Kazuya Takeda,[§] Keiro Shirotani,[‖] Keikichi Takahashi,[§] Kiyoko S. Murayama,* Fuyuki Kametani,[#] Hirohisa Shiraishi, Hiroto Komano,** and Takeshi Tabira[§]**

*Department of Demyelinating Disease and Aging, National Institute of Neuroscience, NCNP, Kodaira, Tokyo, Japan; [†]Katayanagi Advanced Research Laboratories, Tokyo University of Technology, Hachioji, Tokyo, Japan; [‡]Neuroscience Research Institute, Peking University, Beijing, P. R. China; [§]National Institute of Longevity Sciences, NCGG, Obu, Aichi, Japan; [‖]Department of Biochemistry, Hokkaido University Graduate School of Medicine, Sapporo, Japan; [#]Tokyo Institute of Psychiatry, Tokyo Metropolitan Organization for Medical Research, Setagaya, Tokyo, Japan; and **Faculty of Pharmaceutical Sciences, Iwate Medical University, Iwate, Japan

ABSTRACT **Presenilin 1 (PS1) forms the γ-secretase complex with at least three components: nicastrin, APH-1, and PEN-2. This complex mediates intramembrane cleavage of amyloid precursor protein (APP) to generate β-amyloid protein (Aβ) as well as other type 1 transmembrane proteins. Although PS1 mutations linked to familial Alzheimer's disease influence these cleavages, their biological consequences have not been fully understood. In this study, we used mRNA differential display analysis to identify a gene, denoted adoplin-1/ORMDL-1, which displays significantly reduced expression in association with PS1 mutations. Adoplin-1 and two highly homologous genes (adoplin-2, -3) constitute a gene family that encodes transmembrane proteins. The mRNA and protein levels of adoplins (particularly adoplin-1, -2) were markedly elevated in PS-deficient fibroblasts, compared to wild-type cells. Moreover, knockdown of the three adoplins by RNA interference affected maturation of nicastrin and its association with PS1. Adoplin knockdown additionally resulted in elevated levels of APP C-terminal fragments and decreased Aβ production, suggestive of reduced γ-secretase activity. Our data collectively indicate that adoplins are unique molecules with PS-related expression and functions that may play important role(s) in the maturation and activity of the γ-secretase complex.—Araki, W., Takahashi-Sasaki, N., Chui, D.-H., Saito, S., Takeda, K., Shirotani, K., Takahashi, K., Murayama, K. S., Kametani, F., Shiraishi, H., Komano, H., Tabira, T. A family of membrane proteins associated with presenilin expression and γ-secretase function. *FASEB J.* 22, 819–827 (2008)**

Key Words: Alzheimer's disease · β-amyloid · nicastrin

ALZHEIMER'S DISEASE (AD) IS THE MOST common neurodegenerative dementia in the elderly population, characterized pathologically by neuronal and synaptic loss and extensive formation of senile plaques and neurofibrillary tangles. The principal component of senile plaques is β-amyloid protein (Aβ), of which accumulation appears to play a key role in the pathogenesis of AD. Aβ is produced by sequential proteolysis of its precursor, amyloid precursor protein (APP), by β- and γ-secretases. β-Secretase cleavage of APP generates the secreted derivative, sAPP-β, and β-C-terminal fragment, β-CTF. The latter is subsequently cleaved by γ-secretase, yielding Aβ40 and Aβ42. Alternative cleavage of APP by α-secretase generates sAPP-α and α-CTF, precluding Aβ production (1).

Presenilin 1 (PS1) and PS2 genes are linked to autosomal dominant early onset familial AD (2, 3). PS1 or PS2 comprises the catalytic component of PS-γ-secretase, a novel type of aspartyl protease complex composed of at least four membrane proteins, including PS1 or PS2, nicastrin, APH-1, and PEN-2 (4–6). Recent reports that CD147 and TMP21 are regulatory cofactors of the γ-secretase complex (7, 8) have yet to be confirmed clearly. The PS complex catalyzes γ-cleavage of APP within the membrane to generate Aβ. Familial AD-associated PS mutations lead to alterations in the γ-secretase processing of APP to increase the generation of highly amyloidogenic Aβ42, relative to Aβ40 (9). The PS complex is additionally responsible for processing various type 1 membrane proteins, including Notch and cadherins (10), and AD-causing PS mutations influence their cleavage (11–14). Thus, the biological consequences of PS mutations are complicated, and their characterization may aid in improving our understanding of the pathological mechanisms of AD.

In this study, we used mRNA differential display (DD) analysis (15) to identify genes that are differentially expressed in neuronal cells with wild-type PS1 *vs.*

[1] Correspondence: Department of Demyelinating Disease and Aging, National Institute of Neuroscience, NCNP, Kodaira, Tokyo 187-8502, Japan. E-mail: araki@ncnp.go.jp

doi: 10.1096/fj.07-9072com

those with familial AD-associated mutant PS1. We isolated a novel gene (adoplin-1 or ORMDL-1) that is specifically down-regulated in association with PS1 mutations. This gene and two highly homologous genes (adoplin-2 and -3/ORMDL-2 and -3) constitute an evolutionally conserved gene family that encodes integral membrane proteins with unknown functions (16). Our subsequent analyses further indicate that adoplins are unique molecules with PS-related expression and functions.

MATERIALS AND METHODS

Differential display analysis

Total RNA was isolated from wild-type and mutant PS1-transfected SH-SY5Y cells, as described previously (17). To preclude selection bias, total RNA preparations from two different clones were mixed and used for cDNA synthesis with T11VV downstream primers. PCR was performed using multiple primer sets (9 down primers×24 up primers; Takara, Tokyo, Japan) and ^{35}S-dATP. Amplified products were separated on a polyacrylamide gel, followed by autoradiography. DNA recovered from differential display bands on the gel was reamplified using modified primer pairs (extra 8–9 bases were added to the 5′ ends of primers; 18), subcloned into pUC18, and sequenced.

Northern blot analysis

mRNA was extracted with the Poly(A)Pure™ mRNA isolation kit (Ambion, Austin, TX, USA) and further purified with phenol/chloroform. Northern blotting was performed according to a previous report (17). Signals of mRNA were quantified using a BAS5000 image analyzer (Fuji Film Co., Tokyo, Japan). β-actin labeling was used as an internal control to normalize RNA loading.

Cell cultures and transfection

Murine wild-type fibroblasts and PS1-deficient, PS2-deficient, and PS1/PS2-doubly deficient fibroblasts immortalized with a large T antigen were maintained as described previously (19). Wild-type or mutant (I143T or G384A) PS1 cDNA were transfected into SH-SY5Y or H4 cells, and stable transformants were obtained by selection with hygromycin, as described previously (20, 21). Adoplin-1, -2, and -3 cDNA were subcloned into pcDNA3.1 vector (Invitrogen, Carlsbad, CA, USA) and transfected into SH-SY5Y cells. Stable transfectants were selected with G418. SH-SY5Y cells stably transfected with APP were described previously (21). HeLa cells were transfected with "Swedish" mutant APP (swAPP) cDNA, and stable transfectants obtained as above. Notch ΔE cDNA with the C-terminal myc epitope subcloned into pcDNA3 vector was provided by Dr. Raphael Kopan (22). Transient transfection was performed using Lipofectamine 2000 (Invitrogen) or FuGENE6 (Roche, Mannheim, Germany), according to the manufacturer's instructions. Rat primary cerebral cortical neurons were cultured as described previously (23).

Antibodies

Polyclonal rabbit antibodies to adoplin-1 (anti-Adp1) were raised against the synthetic peptide corresponding to residues 134–153 of human adoplin-1 and purified by affinity chromatography on a HiTrap NHS-activated HP column (GE Healthcare Bio-Sciences, Piscataway, NJ, USA) coupled with the peptide. Other antibodies employed include polyclonal anti-PS1-loop (anti-CX against residues 346–363 of human PS1), monoclonal anti-PS1N (24), polyclonal anti-nicastrin (Sigma, St. Louis, MO, USA), anti-APH-1aL (Covance, Berkeley, CA, USA), anti-PEN-2 (provided by Dr. Gopal Thinakaran) (25), anti-APP C-terminal (R37) (26), monoclonal anti-APP N-terminal (Chemicon, Temecula, CA, USA), and anti-myc (Invitrogen).

Western blot analysis

Cells were lysed in RIPA buffer containing protease inhibitors and processed according to a previous report (23). For adoplin analysis, samples containing 100–150 μg protein were immunoprecipitated with anti-Adp1 antibodies. Immunoprecipitated proteins were subjected to Western blotting with the same antibodies. Postmortem human brain tissues were homogenized in 10 mM Tris, pH 8; 150 mM NaCl containing protease inhibitors; and centrifuged at 100,000 *g* for 1 h. The resultant pellet was lysed in RIPA buffer and analyzed as above.

Immunoprecipitation

Cells were lysed in buffer containing 1% CHAPSO and protease inhibitors (27). Lysates were incubated with anti-PS1N covalently attached to protein G-agarose beads. Immunoprecipitated proteins were analyzed by Western blotting with the appropriate antibodies.

Immunohistochemistry

Human brain tissue sections were prepared, and double-immunohistochemical staining was performed following a previously documented method (28). Briefly, sections were incubated with anti-Adp1 and subsequently with FITC-conjugated anti-rabbit IgG. For double-staining, sections were treated with primary antibodies [monoclonal anti-NeuN (Chemicon), anti-glial fibrillary acidic protein (GFAP) (DakoCytomation, Kyoto, Japan), or anti-Aβ (6F/3d, DakoCytomation)], followed by incubation with Texas-Red conjugated anti-mouse IgG. Next, sections were observed with a confocal laser scanning microscope imaging system (FLUOVIEW, Olympus, Tokyo, Japan). Immunocytochemical staining of cultured neurons was performed according to a previous report (23).

RNA interference

Single-stranded gene-specific sense and antisense RNA oligomers were synthesized by Qiagen (Hilden, Germany). The specific siRNA sequences were directed to the following targets: adoplin-1, 5′-ACACAGCTTCTCTCCTGAG-3′; adoplin-2, 5′-AGGCTCGGCTACTGACACA-3′; adoplin-3, 5′-AAGTACGACCAGATCCATT-3′. Control nonsilencing siRNA was obtained from Qiagen. siRNA duplexes were transfected using a HiPerFect transfection reagent (Qiagen), according to the manufacturer's instructions. We used two consecutive rounds of transfection (29). For measurement of secreted Aβ, culture media were changed one day after the second transfection. Cells and conditioned media were harvested the next day. A mixture of siRNAs to adoplin-1, -2, and -3 was used to achieve downregulation of adoplin expression (10 nM each).

Control nonsilencing siRNA was used at a concentration of 30 nM.

Aβ measurement

Aβ1–40 in conditioned media was measured using a sandwich enzyme-linked immunosorbent assay (ELISA) kit (IBL, Gunma, Japan), based on the manufacturer's instructions.

RESULTS

Isolation of the adoplin-1 gene by differential display analysis

Human SH-SY5Y neuroblastoma cells stably transfected with wild-type or familial AD-associated mutant PS1 (I143T or G384A; designated SH-WT PS1, SH-I143T PS1, and SH-G384A PS1, respectively; 20, 21) were used for mRNA DD analysis. The expression levels of PS1 proteins in all transfectants were equivalent (data not shown). After repeated DD experiments, we identified two clones that were down-regulated in both SH-I143T PS1 and SH-G384A PS1 cells, compared to SH-WT PS1 cells. Subsequent sequence analyses revealed that the one clone corresponded to partial ORMDL-1 cDNA (16) and the other to human ribosomal protein L23a cDNA. We isolated full-length cDNA clones of the former gene encoding a protein of 153 amino acid residues (**Fig. 1*A***) and redesignated the gene "adoplin-1" (a down-regulated gene in mutant presenilin 1 cells) for convenience.

Decreased adoplin-1 mRNA expression in mutant PS1-transfected cells was verified by Northern blotting (Fig. 1*B*). Specifically, the adoplin-1 mRNA levels in SH-I143T PS1 and SH-G384A PS1 cells were 36 ± 1 and 33 ± 7% of control SH-WT PS1 cells, respectively. Mutant PS1-associated down-regulation of adoplin-1 mRNA was additionally observed in stably transfected human neuroglioma H4 cells (44 and 59% in H4 cells expressing I143T PS1 and G384A PS1, respectively, compared to H4 cells expressing wild-type PS1). Northern blot analysis of human tissues disclosed adoplin-1 mRNA transcripts in various tissues, including brain, as a major ~1.4 kb band (Fig. 1*C*). Adoplin-1 mRNA was expressed in different subregions of the brain at similar levels (data not shown). Relatively higher mRNA expression was observed in the heart, placenta, and pancreas.

We further found that two paralogs of human adoplin-1/ORMDL-1 exist in the database (designated adoplin-2 and -3/ORMDL-2 and -3) and cloned their cDNAs (16). Adoplin-2 and -3 mRNA were observed ubiquitously (Fig. 1*C*). Interestingly, adoplin-2 and -3 mRNA levels in SH-I143T PS1 and SH-G384A PS1 cells were lower than those in SH-WT PS1 cells (Fig. 1*B*), although their decreases were not as significant as those observed with adoplin-1. Homologous genes to human adoplin-1, -2, and -3 have been identified in mouse, and a single homologue exists in *Drosophila* (Fig. 1*A*). Northern blot analysis of mouse tissues confirmed that the three adoplin genes are expressed ubiquitously (Fig. S1). Weakly homologous genes have additionally been identified in fungi and plants (16). The estimated hydropathy profile of the adoplin-1 protein is depicted in Fig. 1*D*. Hydropathy analysis and the PSORT program (http://psort.nibb.ac.jp) predict that adoplin-1 protein is a type 1b integral membrane protein with one transmembrane region, although its exact transmembrane topology remains unclear at present (Fig. 1*E*; 16). The THWEQ sequence in the middle part of the adoplin sequences is highly conserved among different species and may represent a functionally important region.

Expression of adoplin in neurons

To determine adoplin-1 protein expression, we generated a specific antibody to the C-terminus of human adoplin-1 (anti-Adp1). Western blotting with this antibody allowed the detection of overexpressed and endogenous proteins (~17 kDa) in adoplin-1-transfected SH-SY5Y cells and nontransfected cells, respectively (**Fig. 2*A***). Since the C-terminal region is highly conserved among the three adoplin homologs, the antibody also recognized adoplin-2 and adoplin-3 proteins in cells transfected with the corresponding constructs (Fig. 2*A*, not shown). His-tagged adoplin-1 proteins expressed in *E. coli* displayed a similar molecular weight to those in SH-SY5Y cells (data not shown), implying that no extensive modifications of adoplin-1 occur in mammals. Western blot analysis further showed that endogenous adoplin protein levels in SH-I143T PS1 and SH-G384A PS1 cells were similar to those in SH-WT PS1 cells (data not shown), despite lower adoplin-1 mRNA expression in the former cultures.

We also observed the presence of ~17 kDa adoplin proteins in the membrane but not cytosolic, fractions of primary rat cerebral cortical neurons (data not shown) and human brain tissues (Fig. 2*A*). Immunocytochemical staining of primary cortical neurons showed that adoplin immunoreactivity was localized in both cell bodies and neurites (Fig. 2*B*). Adoplin proteins were primarily expressed in neurons, as evident from immunohistochemical staining of human cerebral cortices of control (data not shown) and AD brains (Fig. 2*C*) with the anti-Adp1 antibody. This finding was further confirmed by double-staining with anti-Adp1 and either anti-NeuN (a marker of neurons) or anti-glial fibrillary acidic protein (GFAP, a marker of astrocytes) (data not shown). Adoplin immunoreactivity did not colocalize with Aβ in senile plaques (Fig. 2*C*). No adoplin immunoreactivity was observed when the primary antibody was replaced with nonimmune rabbit IgG (data not shown). These observations suggest that adoplins are chiefly neuronal proteins.

Increased adoplin expression in PS-deficient cells

The relationship between PS and adoplin was further investigated using PS-deficient cells. We compared the

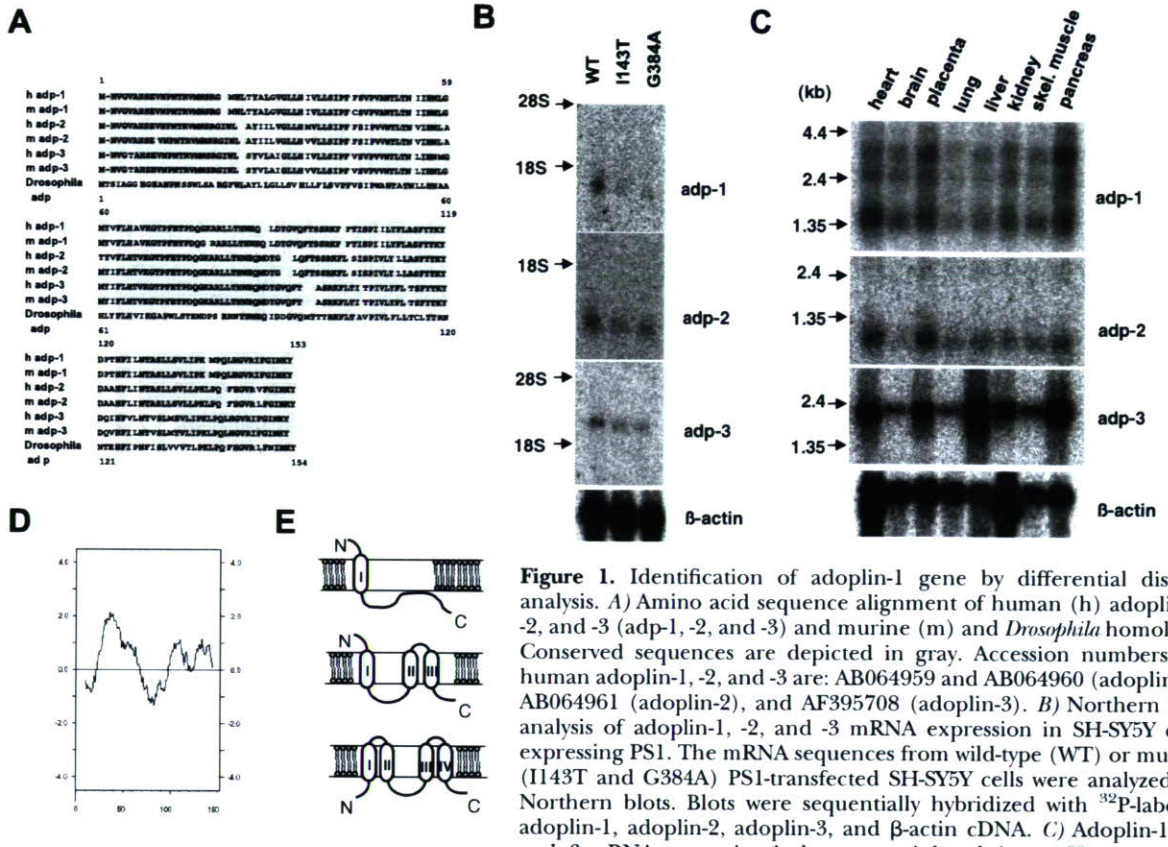

Figure 1. Identification of adoplin-1 gene by differential display analysis. *A)* Amino acid sequence alignment of human (h) adoplin-1, -2, and -3 (adp-1, -2, and -3) and murine (m) and *Drosophila* homologs. Conserved sequences are depicted in gray. Accession numbers for human adoplin-1, -2, and -3 are: AB064959 and AB064960 (adoplin-1), AB064961 (adoplin-2), and AF395708 (adoplin-3). *B)* Northern blot analysis of adoplin-1, -2, and -3 mRNA expression in SH-SY5Y cells expressing PS1. The mRNA sequences from wild-type (WT) or mutant (I143T and G384A) PS1-transfected SH-SY5Y cells were analyzed on Northern blots. Blots were sequentially hybridized with ^{32}P-labeled adoplin-1, adoplin-2, adoplin-3, and β-actin cDNA. *C)* Adoplin-1, -2, and -3 mRNA expression in human peripheral tissues. Human multiple tissue Northern blots (Clontech, Palo Alto, CA, USA) were hybridized with ^{32}P-labeled probes, as in *B. D)* The hydropathy profile of adoplin-1 was plotted using the hydrophobicity indices of Kyte and Doolittle (40), with a window size of 19 residues. The hydropathy profiles of adoplin-2 and -3 are essentially similar to those of adoplin-1. *E)* Models of the possible transmembrane topology of adoplin protein. Three possible models with one, three, or four transmembrane segments are depicted.

adoplin protein levels in fibroblasts derived from wild-type, PS1-deficient, PS2-deficient, and PS1/PS2-doubly deficient mice (19). Interestingly, endogenous adoplin protein expression was increased marginally (~2-fold) in PS1- or PS2-deficient cells and markedly (~6-fold) in PS1/PS2 doubly deficient cells, compared to wild-type cells (**Fig. 3*A*, *B***). Northern blot analyses disclosed that adoplin-1 and -2 mRNA levels were increased by 1.7-fold and 2.0-fold in PS1-deficient cells, 2.5-fold and 2.8-fold in PS2-deficient cells, and 4.7-fold and 6.5-fold in double PS-deficient cells, respectively, relative to wild-type cells; adoplin-3 mRNA levels were similar among the cells examined (Fig. 3*C*, *D*). Immunocytochemical staining with the anti-Adp1 antibody additionally showed that the intensity of adoplin immunoreactivity was higher in PS1/PS2-deficient cells than wild-type cells (data not shown). These data clearly indicate that PS deficiency results in enhanced adoplin-1 and -2 mRNA and protein expression.

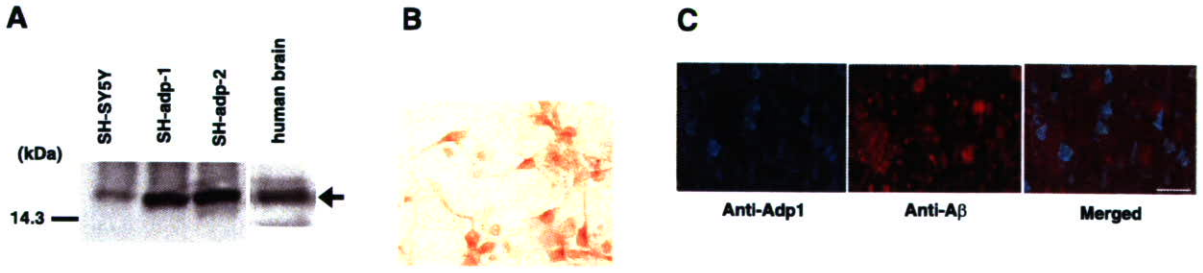

Figure 2. Adoplin protein expression in cultured cells and human brain tissues. *A)* Western blot analysis of adoplin expression in SH-SY5Y cells stably transfected with vector alone, adoplin-1, or adoplin-2, and the membrane fraction of human brain tissues. Anti-Adp1 antibody detected a ~17 kDa protein, as indicated with an arrow. *B)* Immunostaining of primary rat cerebral cortical neurons with anti-Adp1. *C)* Immunohistochemical analysis of adoplin proteins in AD brain tissues. Brain sections were doubly immunostained with anti-Adp1 (green) and anti-Aβ (red), as described in Materials and Methods. Scale bar = 60 μm.

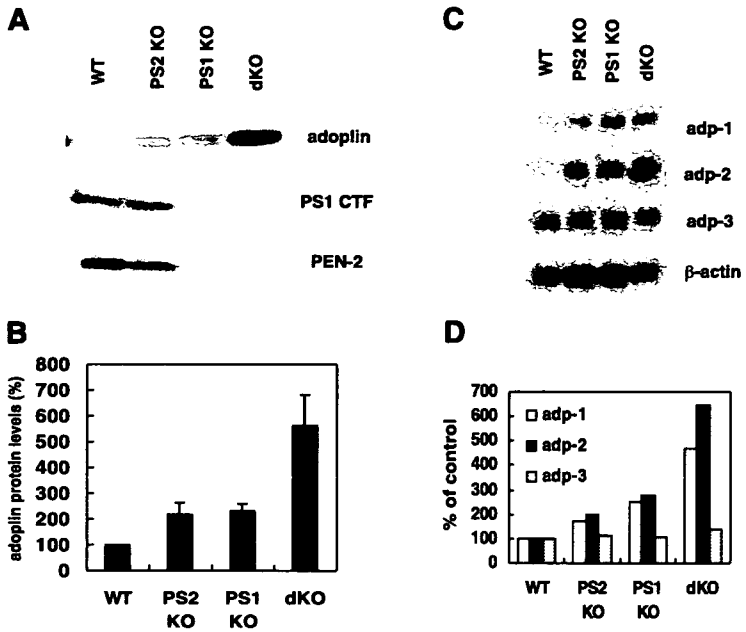

Figure 3. Enhanced expression of adoplin in PS-deficient cells. *A)* Western blot analysis of adoplin expression in wild-type fibroblasts and PS1-deficient (PS1 KO), PS2-deficient (PS2-KO), or PS1/PS2-deficient (dKO) fibroblasts. *B)* Adoplin protein expression levels were quantified, and the relative levels were plotted. Data are presented as means ± SE from three independent experiments. *C)* Northern blot analysis of adoplin-1, -2, and -3 mRNA in wild-type fibroblasts and PS1-, PS2-, or PS1/PS2-deficient fibroblasts. *D)* mRNA levels of adoplin-1, -2, and -3 were quantitated, and relative levels were plotted. Data are presented as means ± SE from three independent experiments.

Adoplin could possibly be a substrate of γ-secretase that accumulates in the absence of PS. To investigate this theory further, we examined the effect of the γ-secretase inhibitor, DAPT (*N*-[*N*-(3,5-difluorophenacetyl)-L-alanyl]-(*S*)-phenylglycine *t*-butyl ester) (30), on adoplin protein expression. Treatment with DAPT did not significantly alter adoplin levels in adoplin-1-expressing cells but led to a marked increase in APP CTF levels in APP-expressing cells (**Fig. 4*A*, *B***). These findings indicate that augmented levels of adoplin proteins in PS-deficient cells do not result from reduced degradation by γ-secretase but from enhanced transcription of adoplin genes.

Adoplin knockdown affects γ-secretase function

To clarify the functional relationship between adoplin proteins and PS1-γ-secretase, we first examined whether adoplin overexpression has any influence on PS complex proteins. The levels of PS1 complex proteins were unaffected in SH-SY5Y cells overexpressing adoplin-1 (**Fig. 5*A***), suggesting that adoplin overexpression does not influence the expression of PS complex proteins.

Next, we performed RNAi experiments using HeLa cells. For downregulation of adoplin protein expression, cells were transfected with three small interfering RNAs (siRNAs) specific for adoplin-1, -2, and -3. As negative controls, cells were transfected with nonsilencing siRNAs. Significant reduction (~80%) in adoplin protein levels was observed following treatment with adoplin siRNAs (Fig. 5*B*). The adoplin siRNAs did not affect cellular viability, although some morphological changes such as thinner cell shape were observed (data not shown). Adoplin knockdown did not affect the expression of endogenous PS1, PS2, APH-1, or PEN-2. However, the levels of the immature nicastrin were significantly augmented (Fig. 5*B*). Densitometric quantification estimated that immature nicastrin levels were increased approximately 2-fold, and mature nicastrin levels were almost unchanged in adoplin siRNA-treated cells compared with control cells (Fig. 5*C*). However, adoplin knockdown did not influence maturation of APP (Fig. 5*B*). Thus, adoplin downregulation appears to specifically impair nicastrin maturation. In these RNAi experiments, nonspecific induction of interferon responses (31) was unlikely because no upregulation of Stat1, one of the interferon-stimulated genes, was observed in siRNA-treated cells on Western blots (data not shown).

We then determined whether siRNA-mediated adoplin suppression affects PS complex formation. CHAPSO extracts of siRNA-treated HeLa cells were immunoprecipitated with monoclonal anti-PS1 antibodies, and PS1-associated proteins were analyzed by Western blot-

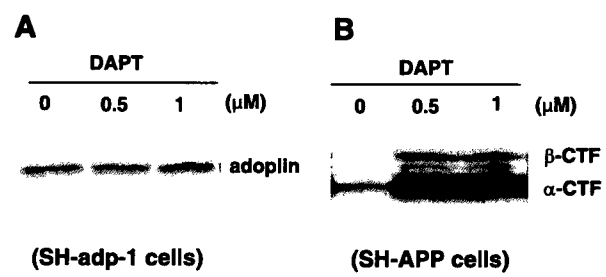

Figure 4. The γ-secretase inhibitor, DAPT, has no effect on adoplin expression. *A)* SH-SY5Y cells stably transfected with adoplin-1 were treated with the indicated concentrations of DAPT for 20 h, followed by Western blot analysis with the anti-Adp antibody. *B)* SH-SY5Y cells stably transfected with APP were treated with DAPT as in *A*, followed by Western blot analysis with an anti-APP antibody. APP α-CTF and β-CTF levels were markedly elevated in DAPT-treated cells.

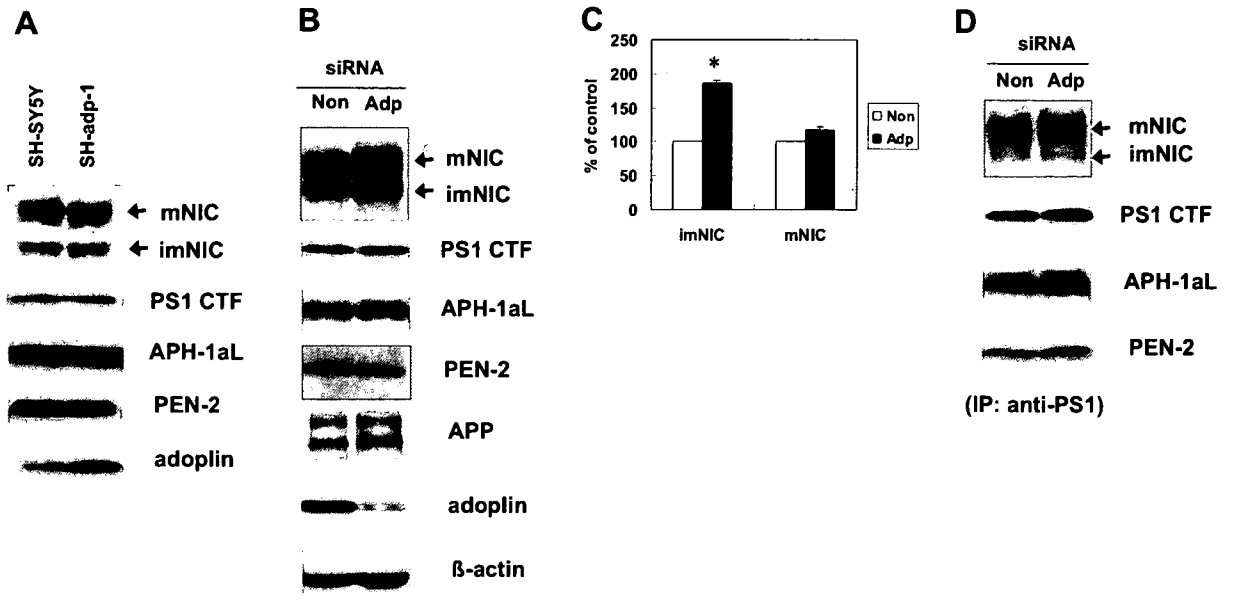

Figure 5. Suppression of adoplin expression causes impaired maturation of nicastrin. *A)* Effects of adoplin overexpression on PS1, nicastrin, APH-1, and PEN-2. Cell lysates of SH-SY5Y and adoplin-1-expressing SH-SY5Y cells were subjected to Western blotting with the relevant antibodies. *B)* Effects of RNAi-mediated suppression of adoplin expression on PS1, PS2, nicastrin, APH-1, and PEN-2. HeLa cells were treated with either nonsilencing (Non) or adoplin (Adp) siRNAs (mixture of siRNAs for three adoplins), as described in Materials and Methods. Cell lysates were subjected to Western blotting with the relevant antibodies. *C)* Immature and mature nicastrin bands from *B* were quantitated, and relative levels were calculated. Data represent means ± SE from three independent experiments. $*P < 0.01$ differed significantly from control by the paired *t* test. *D)* Effects of adoplin suppression on PS1 complex-associated proteins. SiRNA-treated HeLa cells were lysed in buffer containing 1% CHAPSO. PS1 complexes were immunoprecipitated with anti-PS1N antibodies, and immunoprecipitated proteins were analyzed by Western blotting as in *B*. mNIC, mature NIC; imNIC, immature NIC.

ting. Levels of PS1-associated APH-1aL, PEN-2, and PS1 remained almost unchanged in siRNA-treated cells, compared with control cells (Fig. 5*D*). In contrast, significantly less mature nicastrin (~75% of control) was associated with PS1 in adoplin siRNA-treated cells (Fig. 5*D*). Immature nicastrin barely associated with PS1 in both cell types, consistent with previous reports (32, 33). Adoplin proteins did not appear to be in close physical association with PS1 or nicastrin because endogenous adoplin proteins did not coimmunoprecipitate with neither PS1 nor nicastrin (data not shown).

Next, we examined whether downregulation of adoplin affects γ-secretase-mediated cleavage of APP and Notch. In HeLa cells transfected with adoplin siRNAs, a significant (~3 fold) increase in the APP α-CTF level was observed, compared to those transfected with control siRNA (**Fig. 6*A*, *B***). Following transient transfection of APP β-CTF, both β- and α-CTF bands were augmented in these cells (Fig. 6*A*). Furthermore, transient transfection of Notch ΔE (22), the direct substrate of γ-secretase, led to a significant increase in its level while that of Notch intracellular domain (NICD) remained unaltered in adoplin siRNA-treated cells (Fig. 6*C*). The data indicate that γ-secretase cleavage of APP and NotchΔE are inhibited due to loss of adoplin. The effects of adoplin downregulation on Aβ generation were assessed by measuring Aβ levels in conditioned media of HeLa cells stably expressing swAPP. Levels of Aβ1–40 in media from adoplin siRNA-treated cells were decreased to ~40% of that from control cells (Fig. 6*E*). Levels of Aβ1–42 were below detection limits. Since the cellular level of full-length APP remained unaltered (Fig. 6*D*), it is likely that Aβ secretion was suppressed due to inhibition of γ-secretase cleavage of APP. These results suggest that adoplin knockdown affects not only nicastrin maturation but also γ-secretase activity.

DISCUSSION

Familial AD-associated PS mutations alter the γ-cleavage of APP, increasing the ratio of Aβ42 relative to Aβ40, which is a pathologically significant event. Notably, AD-causing PS mutations additionally alter proteolytic function toward several different substrates, such as Notch and cadherins. Thus, the molecular effects of PS mutations are complicated, and some find dispute over the underlying AD-inducing mechanisms (34, 35). In this study, we employed mRNA DD analysis to identify a novel gene, adoplin-1/ORMDL-1, which displays reduced expression in neuronal cells containing mutant PS1 relative to those with wild-type PS1. Adoplin-1 (or ORMDL-1) and two highly homologous genes, adoplin-2 and -3 (or ORMDL-2 and -3), constitute an evolutionally conserved family encoding inte-

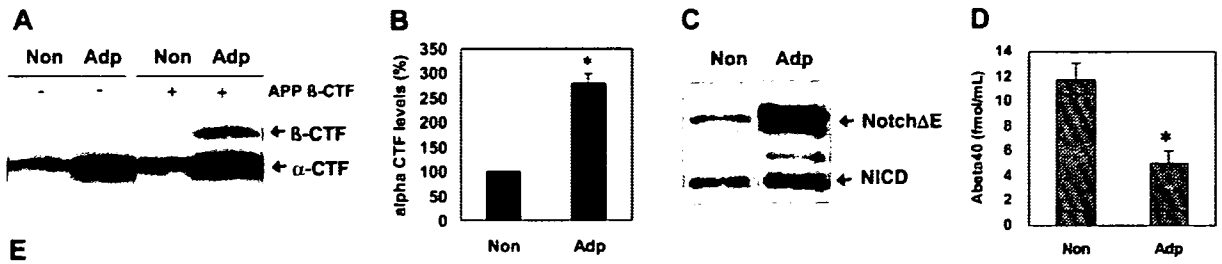

Figure 6. γ-Secretase function is affected by adoplin knockdown. *A)* Effect of adoplin RNAi on cellular levels of APP CTF. HeLa cells were treated with nonsilencing (Non) or adoplin (Adp) siRNAs and were transfected further with APP β-CTF cDNA or vector. APP CTF in cell lysates was analyzed by Western blotting with anti-APP (R37). *B)* α-CTF levels in control and adoplin siRNA-treated cells were quantitated, and relative levels were calculated. Data means ± SE from three independent experiments. $*P < 0.05$ by the paired *t* test. *C)* Effects of adoplin RNAi on Notch cleavage. HeLa cells treated with siRNA were transfected with NotchΔE cDNA, and cell lysates analyzed by Western blotting with anti-myc. *D)* Effects of adoplin suppression on Aβ production. HeLa cells stably expressing swAPP were treated with nonsilencing or adoplin siRNAs, and Aβ1–40 levels in 24 h conditioned media were measured by sandwich ELISA. Data are presented as means ± SE of three independent experiments. $*P < 0.01$ by the paired *t* test. *E)* Cellular APP protein expression in cells used in *C*, as analyzed by Western blotting with anti-APP antibodies. mAPP, mature APP; imAPP, immature APP.

gral membrane proteins of 153 amino acids (Fig. 1*A*). Due to the lack of characteristic functional domains, the physiological functions of adoplins are currently unknown. Expression patterns of these proteins were characterized by using Northern and Western blot analyses and immunohistochemistry. We further investigated the possible relationship between adoplins, PS expression, and γ-secretase function using PS-null cells and RNAi techniques. Unexpectedly, expression of adoplin protein and mRNA was markedly up-regulated in PS-deficient cells. Furthermore, our RNAi experiments revealed that siRNA-mediated adoplin suppression affects nicastrin maturation and PS-γ-secretase activity, thus highlighting its relevance in PS-γ-secretase function.

Northern blot analysis showed that the three adoplin genes are expressed ubiquitously, in keeping with a previous report (16). Adoplin-1 and -2 mRNA expression patterns are different in human and mouse tissues. Specifically, mouse but not human adoplin-1 and -2 transcripts are particularly abundant in the liver and kidney. An antibody specific for the C-terminus of adoplin-1 was employed to determine its expression in cultured neuronal cells and human brain tissues. This antibody is sufficiently sensitive to detect a ~17 kDa endogenous adoplin protein in the membrane fraction on Western blots, although it cannot distinguish among the three homologs. Immunohistochemical analyses disclosed that adoplin proteins are primarily expressed in the neurons of cerebral cortices. Moreover, adoplin is localized mainly in the cell bodies and neurites of primary cortical neurons, which shows possible role(s) in nerve cells. Adoplin immunoreactivity is not colocalized in senile plaques, which suggests that the protein does not function in the extracellular deposition of Aβ.

In contrast to the significant downregulation of adoplin-1 mRNA in mutant PS1-expressing cells, mRNAs of adoplin-1 and -2 are up-regulated moderately in PS1- or PS2-deficient cells and markedly in PS1-/PS2-doubly deficient cells. One possible explanation for this is that adoplin gene expression is under transcriptional control by PS (**Fig. 7**). We postulate that the expression of adoplin-1 and -2 mRNA is maintained at low levels under normal conditions involving regulated PS-associated signaling. Adoplin expression may be controlled *via* signaling pathway(s) downstream of specific γ-secretase substrate(s). Alternatively, Wnt/β-catenin signaling may be involved in the upregulation of adoplins, since PS deficiency results in increased β-catenin stability (36). Our experiments with a γ-secretase inhibitor indicate that adoplin is not a substrate of γ-secretase. Thus, it is unlikely that the significant enhancement in adoplin expression in PS-null cells results from decreased degradation by PS-γ-secretase.

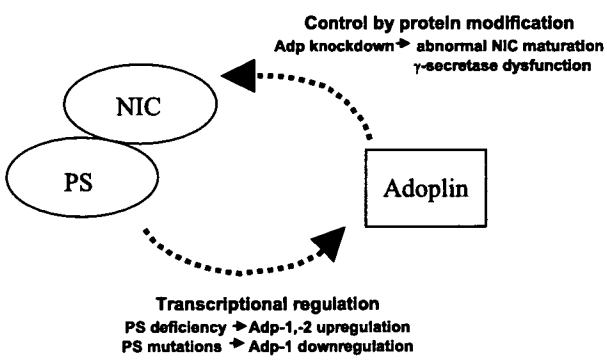

Figure 7. Schema illustrating the relationship between adoplin and PS. Adoplin expression appears to be under transcriptional control by PS. PS deficiency results in the upregulation of adoplin-1 and adoplin-2 mRNA, while familial AD-associated PS mutations lead to down-regulation of adoplin-1 mRNA. However, adoplin knockdown induces abnormal maturation of nicastrin, as well as reduced γ-secretase function. Abnormal nicastrin maturation may be directly associated with the γ-secretase dysfunction, although the precise underlying mechanism remains unclear.

The mechanism underlying mutant PS1-associated downregulation of adoplin-1 is yet to be established but may be a result of gain-of-function, as suggested in a previous microarray study (37). A number of genes were identified that exhibit reverse-expression alterations in the brains of PS1 conditional knockout mice and mutant PS1 transgenic mice. The authors suggest that the familial AD-linked PS1 variant produces transcriptome changes primarily by gain of aberrant function (37). We did not observe a clear reduction in adoplin protein expression in mutant PS1-expressing cells despite the significant downregulation of adoplin-1 mRNA. The reason for this discrepancy is unclear. It is possible that the extent of downregulation of adoplin-1 is not sufficiently large to alter total adoplin protein expression.

Our RNAi experiments show that adoplin knockdown does not affect the expression of endogenous PS1, APH-1, and PEN-2 but significantly influences nicastrin maturation. The level of immature nicastrin is clearly augmented by adoplin knockdown. This effect appears specific, since maturation of APP remains unaffected. Importantly, significantly less mature nicastrin is associated with PS1 in adoplin knockdown cells than control cells, suggesting disruption of PS complex formation. Furthermore, loss of adoplin results in decreased γ-secretase cleavage of APP and Notch (as indicated by accumulation of APP CTF and Notch ΔE) and reduced Aβ production, implying significantly reduced γ-secretase activity. Nicastrin plays a critical role in maintaining the PS-γ-secretase complex and serving as a γ-secretase substrate receptor (38, 39). Thus, impaired nicastrin maturation may be directly associated with the apparent reduction in γ-secretase activity following adoplin knockdown (Fig. 7). However, the possibility that adoplin suppression affects γ-secretase function by a different unknown mechanism cannot be eliminated. A previous study demonstrates that adoplin/ORMDL proteins localize in endoplasmic reticulum membranes (16). Consistent with this report, our preliminary data of biochemical subcellular fractionation indicate that adoplin mainly localizes in the endoplasmic reticulum, where it coresides with PS1, PS2, nicastrin, APH-1, and PEN-2 (data not shown). Experiments using yeast knockout strains also suggest that adoplin/ORMDL functions in correct protein folding and/or trafficking in the endoplasmic reticulum (16). Adoplin may participate in nicastrin trafficking in the endoplasmic reticulum. However, since neither PS1 nor nicastrin coprecipitate with endogenous adoplin, close interactions between adoplin and these proteins appear unlikely. Thus, further research is required to elucidate the mechanism of adoplin action in nicastrin maturation.

We have identified adoplin/ORMDL genes whose transcription is possibly regulated by PS. Our data additionally indicate that adoplins are relevant in PS-γ-secretase function. Thus, adoplins are unique molecules that display PS-related expression and function. In view of the reduced γ-secretase activity following adoplin knockdown, we hypothesize that adoplin may be a therapeutic target for AD. Further clarification of the role(s) of adoplins in relation to PS-γ-secretase may aid in the development of novel therapeutic strategies for AD.

We sincerely thank Drs. Naoyuki Iwabe and Takashi Miyata for estimation of hydropathy; Dr. Raphael Kopan for Notch ΔE cDNA; Dr. Gopal Thinakaran for anti-PEN-2; Dr. Bart De Strooper for PS1-, PS2-, and PS1/PS2-deficient fibroblasts and wild-type fibroblasts; Dr. Masayasu Okochi for HeLa cells; and Dr. Hirohiko Hohjoh for helpful suggestions. This work was supported in part by a grant-in-aid for scientific research from the Ministry of Education, Culture, Sports, Science and Technology of Japan and by grants from the Ministry of Health, Labor, and Welfare of Japan and the Organization for Pharmaceutical Safety and Research.

REFERENCES

1. Selkoe, D. J. (2002) Deciphering the genesis and fate of amyloid beta-protein yields novel therapies for Alzheimer's disease. *J. Clin. Inv.* **110,** 1375–1381
2. Sherrington, R., Rogaev, E. I., Liang, Y., Rogaeva, E. A., Levesque, G., Ikeda, M., Chi, H., Lin, C., Li, G., Holman, K., Tsuda, T., Mar, L., Foncin, J.-F., Bruni, A. C., Montesi, M. P., Sorbi, S., Rainero, I., Pinessi, L., Ne, L., Chumakov, I., Pollen, D., Brookes, A., Sanseau, P., Polinsky, R. J., Wasco, W., Dasilva, H. A., Haines, J. L., Pericak-Vance, M. A., Tanzi, R. E., Roses, A. D., Fraser, P. E., Rommens, J. M., and St. George-Hyslop, P. H. (1995) Cloning of a gene bearing missense mutations in early-onset familial Alzheimer's disease. *Nature* **375,** 754–760
3. Levy-Lahad, E., Wasco, W., Poorkaj, P., Romano, D. M., Oshima, J., Pettingell, W. H., Yu, C.-E., Jondro, P. D., Schmidt, S. D., Wang, K., Crowley, A. C., Fu, Y.-H., Guenette, S. Y., Galas, D., Nemens, E., Wijsman, E. M., Bird, T. D., Schellenberg, G. D., and Tanzi, R. E. (1995) Candidate gene for the chromosome 1 familial Alzheimer's disease locus. *Science* **269,** 973–977
4. Kimberly, W. T., LaVoie, M. J., Ostaszewski, B. L., Ye, W., Wolfe, M. S., and Selkoe, D. J. (2003) Gamma-secretase is a membrane protein complex comprised of presenilin, nicastrin, Aph-1, and Pen-2. *Proc. Natl. Acad. Sci. U. S. A.* **100,** 6382–6387
5. Takasugi, N., Tomita, T., Hayashi, I., Tsuruoka, M., Niimura, M., Takahashi, Y., Thinakaran, G., and Iwatsubo, T. (2003) The role of presenilin cofactors in the gamma-secretase complex. *Nature* **422,** 438–441
6. Edbauer, D., Winkler, E., Regula, J. T., Pesold, B., Steiner, H., and Haass, C. (2003) Reconstitution of gamma-secretase activity. *Nat. Cell Biol.* **5,** 486–488
7. Zhou, S., Zhou, H., Walian, P. J., and Jap, B. K. (2005) CD147 is a regulatory subunit of the gamma-secretase complex in Alzheimer's disease amyloid beta-peptide production. *Proc. Natl. Acad. Sci. U. S. A.* **102,** 7499–7504
8. Chen, F., Hasegawa, H., Schmitt-Ulms, G., Kawarai, T., Bohm, C., Katayama, T., Gu, Y., Sanjo, N., Glista, M., Rogaeva, E., Wakutani, Y., Pardossi-Piquard, R., Ruan, X., Tandon, A., Checler, F., Marambaud, P., Hansen, K., Westaway, D., St George-Hyslop, P., and Fraser, P. (2006) TMP21 is a presenilin complex component that modulates gamma-secretase but not epsilon-secretase activity. *Nature* **440,** 1208–1212
9. Sisodia, S. S., and St. George-Hyslop, P. H. (2002) gamma-Secretase, Notch, Abeta, and. Alzheimer's disease: where do the presenilins fit in? *Nat. Rev. Neurosci.* **3,** 281–290
10. Wolfe, M. S., and Kopan, R. (2004) Intramembrane proteolysis: theme and variations. *Science* **305,** 1119–1123
11. Song, W., Nadeau, P., Yuan, M., Yang, X., Shen, J., and Yankner, B. A. (1999) Proteolytic release and nuclear translocation of Notch-1 are induced by presenilin-1 and impaired by pathogenic presenilin-1 mutations. *Proc. Natl. Acad. Sci. U. S. A.* **96,** 6959–6963

12. Chen, F., Gu, Y., Hasegawa, H, Ruan, X., Arawaka, S., Fraser, P., Westaway, D., Mount, H., and St. George-Hyslop, P. (2002) Presenilin 1 mutations activate gamma 42-secretase but reciprocally inhibit epsilon-secretase cleavage of amyloid precursor protein (APP) and S3-cleavage of notch. *J. Biol. Chem.* **277,** 36521–36526
13. Marambaud, P., Wen, P. H., Dutt, A., Shioi, J., Takashima, A., Siman, R., and Robakis, N. K. (2003) A CBP binding transcriptional repressor produced by the PS1/epsilon-cleavage of N-cadherin is inhibited by PS1 FAD mutations. *Cell* **114,** 635–645
14. Bentahir, M., Nyabi, O., Verhamme, J., Tolia, A., Horre, K., Wiltfang, J., Esselmann, H., and De Strooper, B. (2006) Presenilin clinical mutations can affect gamma-secretase activity by different mechanisms. *J. Neurochem.* **96,** 732–742
15. Liang, P., and Padree, A. B. (1992) Differential display of eukaryotic messenger RNA by means of the polymerase chain reaction. *Science* **257,** 967–971
16. Hjelmqvist, L., Tuson, M., Marfany, G., Herrero, E., Balcells, S., and Gonzalez-Duarte, R. (2002) ORMDL proteins are a conserved new family of endoplasmic reticulum membrane proteins. *Genome Biol.* **3,** RESEARCH0027
17. Lee, R. K., Araki, W., and Wurtman, R. J. (1997) Stimulation of amyloid precursor protein synthesis by adrenergic receptors coupled to cAMP formation. *Proc. Natl. Acad. Sci. U. S. A.* **94,** 5422–5426
18. Wang, X., and Feuerstein, G. Z. (1995) Direct sequencing of DNA isolated from mRNA differential display. *BioTechniques* **18,** 448–452
19. Herreman, A., Serneels, L., Annaert, W., Collen, D., Schoonjans, L., and De Strooper, B. (2000) Total inactivation of gamma-secretase activity in presenilin-deficient embryonic stem cells. *Nat. Cell Biol.* **2,** 461–462
20. Shirotani, K., Takahashi, K., and Tabira, T. (1999) Effects of presenilin N-terminal fragments on production of amyloid beta peptide and accumulation of endogenous presenilins. *Neurosci. Lett.* **262,** 37–40
21. Takeda, K., Araki, W., and Tabira, T. (2004) Enhanced generation of intracellular Abeta42 amyloid peptide by mutation of presenilins PS1 and PS2. *Eur. J. Neurosci.* **19,** 258–264
22. Schroeter, E. H., Kisslinger, J. A., and Kopan, R. (1998) Notch-1 signalling requires ligand-induced proteolytic release of intracellular domain. *Nature* **393,** 382–386
23. Araki, W., Yuasa, K., Takeda, S., Takeda, K., Shirotani, K., Takahashi, K., and Tabira, T. (2001) Pro-apopototic effect of presenilin 2 (PS2) overexpression is associated with down-regulation of Bcl-2 in cultured neurons. *J. Neurochem.* **79,** 1161–1168
24. Shirotani, K., Takahashi, K., Araki, W., Maruyama, K., and Tabira, T. (2000) Mutational analysis of intrinsic regions of presenilin 2 that determine its endoproteolytic cleavage and pathological function. *J. Biol. Chem.* **275,** 3681–3686
25. Luo, W. J., Wang, H., Li, H., Kim, B. S., Shah, S., Lee, H. J., Thinakaran, G., Kim, T. W., Yu, G., and Xu, H. (2003) PEN-2 and APH-1 coordinately regulate proteolytic processing of presenilin 1. *J. Biol. Chem.* **278,** 7850–7854
26. Kametani, F., Tanaka, K., Ishii, T., Ikeda, S., Kennedy, H. E., and Allsop, D. (1993) Secretory form of Alzheimer amyloid precursor protein 695 in human brain lacks beta/A4 amyloid immunoreactivity. *Biochem. Biophys. Res. Commun.* **191,** 392–398
27. Saito, S., Takahasi-Sasaki, N., and Araki, W. (2005) Identification and characterization of a novel human APH-1b splice variant lacking exon 4. *Biochem. Biophys. Res. Commun.* **330,** 1068–1072
28. Chui, D.-H., Dobo, E., Makifuchi, T., Akiyama, H., Kawakatsu, S., Petit, A., Checler, F., Araki, W., Takahashi, K., and Tabira, T. (2001) Apoptotic neurons in Alzheimer's disease frequently show intracellular Abeta42 labeling. *J. Alzheimers Dis.* **3,** 231–239
29. Saito, S., and Araki, W. (2005) Expression profiles of two human APH-1 genes and their roles in the formation of presenilin complexes. *Biochem. Biophys. Res. Commun.* **327,** 18–22
30. Dovey, H. F., John, V., Anderson, J. P., Chen, L. Z., de Saint Andrieu, P., Fang, L. Y., Freedman, S. B., Folmer, B., Goldbach, E., Holsztynska, E. J., Hu, K. L., Johnson-Wood, K. L., Kennedy, S. L., Kholodenko, D., Knops, J. E., Latimer, L. H., Lee, M., Liao, Z., Lieberburg, I. M., Motter, R. N., Mutter, L. C., Nietz, J., Quinn, K. P., Sacchi, K. L., Seubert, P. A., Shopp, G. M., Thorsett, E. D., Tung, J. S., Wu, J., Yang, S., Yin, C. T., Schenk, D. B., May, P. C., Altstiel, L. D., Bender, M. H., Boggs, L. N., Britton, T. C., Clemens, J. C., Czilli, D. L., Dieckman-McGinty, D. K., Droste, J. J., Fuson, K. S., Gitter, B. D., Hyslop, P. A., Johnstone, E. M., Li, W. Y., Little, S. P., Mabry, T. E., Miller, F. D., and Audia, J. E. (2001) Functional gamma-secretase inhibitors reduce beta-amyloid peptide levels in brain. *J. Neurochem.* **76,** 173–181
31. Sledz, C. A., Holko, M., de Veer, M. J., Silverman, R. H., and Williams, B. R. (2003) Activation of the interferon system by short-interfering RNAs. *Nat. Cell Biol.* **5,** 834–839
32. Yu, G., Nishimura, M., Arawaka, S., Levitan, D., Zhang, L., Tandon, A., Song, Y. Q., Rogaeva, E., Chen, F., Kawarai, T., Supala, A., Levesque, L., Yu, H., Yang, D. S., Holmes, E., Milman, P., Liang, Y., Zhang, D. M., Xu, D. H., Sato, C., Rogaev, E., Smith, M., Janus, C., Zhang, Y., Aebersold, R., Farrer, L. S., Sorbi, S., Bruni, A., Fraser, P., and St George-Hyslop, P. (2000) Nicastrin modulates presenilin-mediated notch/glp-1 signal transduction and betaAPP processing. *Nature* **407,** 48–54
33. Yang, D. S., Tandon, A., Chen, F., Yu, G., Yu, H., Arawaka, S., Hasegawa, H., Duthie, M., Schmidt, S. D., Ramabhadran, T. V., Nixon, R. A., Mathews, P. M., Gandy, S. E., Mount, H. T., St George-Hyslop, P., and Fraser, P. E. (2002) Mature glycosylation and trafficking of nicastrin modulate its binding to presenilins. *J. Biol. Chem.* **277,** 28135–28142
34. De Strooper, B. (2007) Loss-of-function presenilin mutations in Alzheimer disease. Talking Point on the role of presenilin mutations in Alzheimer disease. *EMBO Rep.* **8,** 141–146
35. Wolfe, M. S. (2007) When loss is gain: reduced presenilin proteolytic function leads to increased Abeta42/Abeta40. Talking Point on the role of presenilin mutations in Alzheimer disease. *EMBO Rep.* **8,** 136–140
36. Xia, X., Qian, S., Soriano, S., Wu, Y., Fletcher, A. M., Wang, X. J., Koo, E. H., Wu, X., and Zheng, H. (2001) Presenilin 1 negatively regulates beta-catenin/T cell factor/lymphoid enhancer factor-1 signaling independently of beta-amyloid precursor protein and notch processing. *Proc. Natl. Acad. Sci. U. S. A.* **98,** 10863–10868
37. Mirnics, K., Korade, Z., Arion, D., Lazarov, O., Unger, T., Macioce, M., Sabatini, M., Terrano, D., Douglass, K. C., Schor, N. F., and Sisodia, S. S. (2005) Presenilin-1-dependent transcriptome changes. *J. Neurosci.* **25,** 1571–1578
38. Shah, S., Lee, S. F., Tabuchi, K., Hao, Y. H., Yu, C., LaPlant, Q., Ball, H., Dann, C. E. 3rd, Sudhof, T., and Yu, G. (2005) Nicastrin functions as a gamma-secretase-substrate receptor. *Cell* **122,** 435–447
39. Zhang, Y. W., Luo, W. J., Wang, H., Lin, P., Vetrivel, K. S., Liao, F., Li, F., Wong, P. C., Farquhar, M. G., Thinakaran, G., and Xu, H. (2005) Nicastrin is critical for stability and trafficking but not association of other presenilin/gamma-secretase components. *J. Biol. Chem.* **280,** 17020–17026
40. Kyte, J., and Doolittle, R. F. (1982) A simple method for displaying the hydropathic character of a protein. *J. Mol. Biol.* **57,** 105–132

Received for publication June 28, 2007.
Accepted for publication September 6, 2007.

Laboratory Animals

Vet Pathol 45:67–72 (2008)

BRIEF COMMUNICATIONS and CASE REPORTS

Transthyretin Amyloidosis and Two Other Aging-Related Amyloidoses in an Aged Vervet Monkey

S. NAKAMURA, S. OKABAYASHI, N. AGEYAMA, H. KOIE, T. SANKAI, F. ONO, K. FUJIMOTO, AND K. TERAO

The Corporation for Production and Research of Laboratory Primates, Tsukuba, Ibaraki, Japan (SN, SO, FO, KF); Tsukuba Primate Research Center, National Institute of Biomedical Innovation, Tsukuba, Ibaraki, Japan (NA, TS, KT); and the Department of Veterinary Medicine, College of Bioscience, Nihon University, Fujisawa, Kanagawa, Japan (HK)

Abstract. An aged male vervet monkey showed severe cardiac arrhythmia for more than 3 years. A multifocal amyloid consisting of transthyretin was deposited in all areas of the heart wall, especially in the extracellular stroma among muscle fibers and external tunica of arterioles. Moreover, the amyloid was deposited in the stroma and arterioles of other systemic organs except the liver and spleen. These characteristics are consistent with senile systemic amyloidosis in humans. A second amyloid consisting of amyloid β protein was in senile plaques and cerebral amyloid angiopathy in the cerebral cortex. A third amyloid consisting of islet amyloid polypeptide was deposited in islets of the pancreas. Apolipoprotein E and amyloid P component colocalized with the 3 amyloids. Thus, 3 different aging-related amyloids were found in an aged vervet monkey. In particular, to our knowledge, this is the first report on spontaneous transthyretin amyloidosis in animals.

Key words: Amyloidosis; amyloid β protein; IAPP; transthyretin.

Amyloid is a degenerative protein that exhibits common biochemical and morphologic characteristics, such as 1) birefringence under polarizing microscope, 2) abundant β pleated-sheets in the secondary structure of the proteins, and 3) nonbranching and nonparallel straight fibrils (8–10 nm in diameter) under electron microscope.[13] However, each amyloid consists of different precursor proteins.[13] Furthermore, amyloidosis may develop secondary to various conditions, such as inflammation, aging, and certain neoplasms. Transthyretin (TTR), amyloid β protein (Aβ), and islet amyloid polypeptide (IAPP) amyloidoses are well known as major aging-related amyloidoses.[15] Among these amyloids, senile systemic amyloidosis (SSA), which is characterized by the deposition of amyloid fibrils containing TTR, is well known in aged humans but not in animals. In SSA, first small amyloid deposits, mainly in the heart, occur without obvious symptoms. However, in some case, massive amyloid deposits result in heart failure, eventually leading to death.[15]

In nonhuman primates, limited literature on amyloidosis is available. However, cerebral Aβ and islet amylin amyloidoses have been investigated in nonhuman primates as models for Alzheimer's disease and diabetes mellitus, respectively.[7,10] In the vervet monkey, there has only been one report on cerebral Aβ deposition preventable by Aβ vaccination,[4] whereas no study has been conducted for other types of amyloidoses.

A male vervet monkey (*Cercopithecus aethiops*), assumed to be 29 years old, showed severe cardiac arrhythmia for more than 3 years and bradycardia at the later stage of the 3 years, which were detected by 4-leads electrocardiography. Premature ventricular contractions (PVCs) were monitored by 24-hour Holter electrocardiography. The frequency of PVCs gradually became severe (3,000 PVCs per day) during the 3 years. Moreover, dilatation of the right ventricle was detected by ultrasound and X-ray examinations. However, for the left ventricle, no obvious disorders, such as reduced left ventricular ejection fractions, were observed by echocardiography. Symptoms associated with Alzheimer's disease and diabetes mellitus were not observed in the present case. Finally, the monkey was euthanized because of poor prognosis due to severe depression and anorexia.

At necropsy, collected tissues were fixed in 10% buffered formalin, embedded in paraffin, and sectioned at 4 μm. The deparaffinized sections were stained with hematoxylin and eosin. Some sections were stained with Congo red and direct fast scarlet (DFS; Muto, Tokyo,